Review

Visible light driven redox-mediator-free dual semiconductor photocatalytic systems for pollutant degradation and the ambiguity in applying Z-scheme concept

Thillai Sivakumar Natarajan[a,b], K. Ravindranathan Thampi[a,*], Rajesh J. Tayade[b,*]

[a] UCD School of Chemical and Bioprocess Engineering, UCD College of Engineering & Architecture, University College Dublin (UCD), Belfield, Dublin 4, Ireland
[b] Inorganic Materials and Catalysis Division, CSIR-Central Salt and Marine Chemicals Research Institute (CSIR-CSMCRI), Gijubhai Badheka Marg, Bhavnagar 364 002, Gujarat, India

A B S T R A C T

Semiconductor photocatalysis using single or modified semiconductors and heterojunction-type composites is limited due to lower visible light response, rapid recombination of photogenerated charge carriers and low redox potentials of photoactive materials. Recently the coordinated applications of two or more semiconductors are becoming popular, an idea borrowed from the thermodynamically uphill driven tandem Z-scheme concept used for photoelectrochemical splitting of water involving two different semiconductors with improved overall visible light response. Consequently, in thermodynamically downhill photocatalytic reactions for pollutant degradation involving dual semiconductors as well the word "Z-scheme" is being used to explain the observed efficient electron-hole separation mechanism. Whereas the Z-scheme classically represents only thermodynamically up-hill photosynthetic reactions ($\Delta G > 0$), the photocatalytic degradation of pollutants, on the other hand, are thermodynamically downhill reactions ($\Delta G < 0$), and this usage is creating a misconception and ambiguity in the field of photocatalysis. Therefore, herein we discuss the principles of the often called 'Z-scheme photosystems' involving (i) shuttle redox-mediators, (ii) dual semiconductors photocatalysts with solid state electron mediators and (iii) redox-mediator-free direct systems. The review relevantly summarizes and discusses various representative dual semiconductor photocatalytic systems with solid state mediators as well as non-mediated direct dual semiconductor photocatalysts studied for the degradation of pollutants under visible light irradiation. The future requirements for the development of an efficient visible light driven redox-mediator-free and durable direct dual semiconductor photocatalytic system for the degradation of pollutants is also presented.

1. Introduction

Many new and effective decomposition techniques such as physical, chemical, thermal, biological and advanced oxidation processes (AOPs) are currently being developed or investigated to clean-up the polluted water and air [1–3]. Among these, AOPs are highly attractive and uses hydroxyl radicals (·OH) as an oxidizing agent. Even though photocatalysis and the generation of peroxides through that method have been widely studied in 1950s [4], the pioneering work of photoelectrochemical water splitting using TiO_2 electrode by Fujishima and Honda in 1972 [5] has added an impetus to the field of photocatalytic decomposition of pollutants. The sustainable use of solar energy in such systems makes the process advantageous. Therefore, semiconductor photocatalysis is recognized as a potential technique to degrade a wide range of pollutants at ambient pressure and temperature into less harmful products and possibly hydrogen from waste waters and subsequent reduction of carbon dioxide (CO_2) into fuels [6–12].

Different types of reactors based on direct sunlight, artificial UV light and light emitting diodes (LEDs) [13–23] have been reported for semiconductor photocatalysis. Semiconductors such as TiO_2, ZnO,
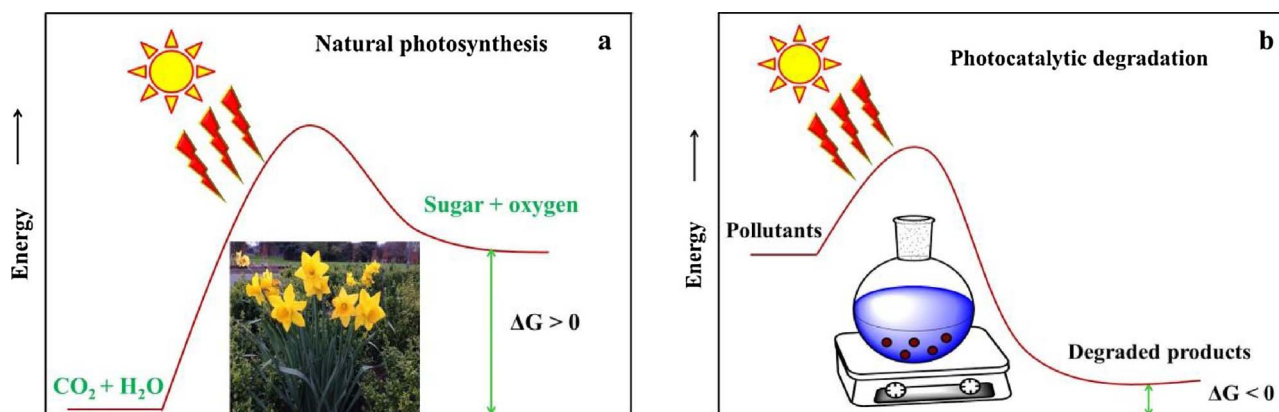
Fig 1. Energy profile diagram for natural photosynthesis by green plants and photocatalytic degradation of pollutants. (For interpretation of the references to colour in this figure legend, the reader is referred to the web version of this article.)

ZrO_2, WO_3, V_2O_5 etc., have been widely used as photocatalysts for the degradation of dyes, pharmaceuticals and other organic pollutants. Among these, the inexpensive TiO_2 is most popular because of its high stability, activity, biocompatibility and eco-friendliness. However, TiO_2 absorbs only UV fraction of the solar spectrum and faces a poor separation of photogenerated charge carriers resulting in dismal reaction efficiencies. Therefore, remarkable improvements have been put forward to tune the bandgap of TiO_2 and decrease the rate of electron-hole pair recombination by doping, through dye-sensitization, and application of graphene and composites [24–33]. However, all efforts fall short of industrial and practical application requirements. From this viewpoint, the non-TiO_2 based visible light active photocatalytic systems such as CdS, graphitic carbon nitride (g-C_3N_4), MoS_2, bismuth catalysts, $ZnIn_2S_4$, ferrites, Ag_3PO_4, Fe_2O_3 etc., have been broadly studied for the degradation of pollutants [34–38]. Though these photocatalysts possess low band gaps for efficient harvesting of visible light, their low stability under reaction conditions and the high rate of photo-excited charge carrier recombination defeats the purpose. Moreover, their valence band (VB) and conduction band (CB) potentials are lower than the potential required to generate reactive hydroxyl radical (H_2O or $-OH/\cdot OH = +2.4$ eV vs. NHE) and superoxide radical anions ($O_2/O_2\cdot^- = -0.33$ eV vs. NHE), which directly take part in the oxidation process.

For efficient visible light induced photocatalysis, the semiconductors should possess lower band gaps, diminished charge recombination rates and more positive VB and negative CB potentials. However, a single photocatalyst with lower band gap cannot simultaneously diminish charge recombination rates and exhibit high redox ability or vice-versa. To overcome this constraint, recently, heterojunction photocatalytic systems involving TiO_2 (CdS/TiO_2, g-C_3N_4/TiO_2, Bi_2WO_6/TiO_2, $BiVO_4$/TiO_2, $ZnFe_2O_4$/TiO_2, etc.) and non-TiO_2 (g-C_3N_4/CdS, Bi_2O_3/Bi_2WO_6, $BiOBr$/g-C_3N_4, $ZnFe_2O_4$/g-C_3N_4, g-C_3N_4/Bi_2WO_6, CdS/Bi_2MoO_6, Bi_2MoO_6/$BiVO_4$, etc.) semiconductor pairs have been developed [32,39–47]. However, the redox potentials of separated photogenerated charge carriers on the conduction and valence bands of two different narrow bandgap semiconductors remain lower, leading to poor generation of reactive radicals and hence decreased reaction rates. These difficulties will have to be addressed to achieve improved visible light photocatalytic efficiencies. Despite intense research in this area spanning over 6 decades, the progress towards attaining practical photocatalytic AOP applications remain elusive.

Recently, the artificial Z-scheme photosystems, which mimic the natural photosynthesis of green plants (photosystem II (PS II) and photosystem I (PS I)) have been developed for water splitting reaction [48]. The natural photosynthesis involves a complex two photon-excitation process generating sufficient potential difference required to

carry forward the reactions, which effectively involves the splitting of water as a key step. Analogously, the artificial Z-scheme photosynthetic systems for water splitting consist of two semiconductors in the presence of suitable redox-mediators (IO_3^-/I^-, Fe^{3+}/Fe^{2+}, NO_3^-/NO_2^-, etc.,), in which the photogenerated electrons and holes are eventually placed in two-separate semiconductors with higher net CB and VB potentials for effecting water reduction and oxidation reactions [49–55]. Since charge carrier transfers in Z-scheme photosystem is achieved through an appropriate redox-mediator, the net energy conversion efficiency relies on the suitability and stability of the redox-mediators, as well. If the redox-mediators strongly absorb visible light photons, then the visible light absorption by semiconductors is compromised and the undesirable backward reactions could decline the hydrogen production efficiency.

Different dual semiconductors photocatalysts with solid-state electron mediators such as metals, reduced graphene oxide (RGO) and carbon, and redox-mediator-free systems have been developed for degradation of pollutants to overcome some of the aforementioned issues [56–62]. They revealed that photogenerated electron hole pairs are efficiently separated in this manner and named the system as Z-scheme with solid-state electron mediators and direct Z-scheme without mediators. However, the experimental evidence for the suggested mechanisms is ambiguous and has not been investigated deeply. The Z-scheme characterizes only thermodynamically uphill reactions (Fig. 1a), for example water splitting reaction, whereas the photocatalytic degradation of pollutants is thermodynamically downhill (Fig. 1b). This variance in understanding the process might create misconception and ambiguity in the usage of "Z-scheme" methods [63]. Therefore, in the forthcoming sections we refer to the mistakenly called Z-scheme photocatalytic systems consisting of solid-state electron mediators as 'dual semiconductor systems with solid-state electron mediators', and those without redox-mediators as 'direct dual semiconductor system' only and avoid using the term 'Z-scheme' photocatalysis.

Dual semiconductor systems with solid-state electron mediators (CdS-Au-TiO_2, Ag/AgBr/TiO_2, AgBr/Ag/Bi_2WO_6) have been developed for degradation of organic pollutants. However, the mediators such as Au, Ag or graphene etc., show absorption of visible light through surface plasmon resonance effect (SPR), leading to decrease in the quantity of light reaching the actual photocatalyst surface [56–58]. Therefore, recently redox-mediator-free direct dual semiconductor photocatalytic systems ($CaFe_2O_4$/WO_3, $CuBi_2O_4$/WO_3, $NaNbO_3$/WO_3, g-C_3N_4/TiO_2) have been prepared and tested to circumvent this problem [59–62]. In this case, the photogenerated charge carriers showed better separation by transferring the electron from CB of the semiconductor 2 to VB of the semiconductor 1 allowing the intended recombination with the holes. Thus, the electrons and holes on the CB and VB of the semiconductor 1
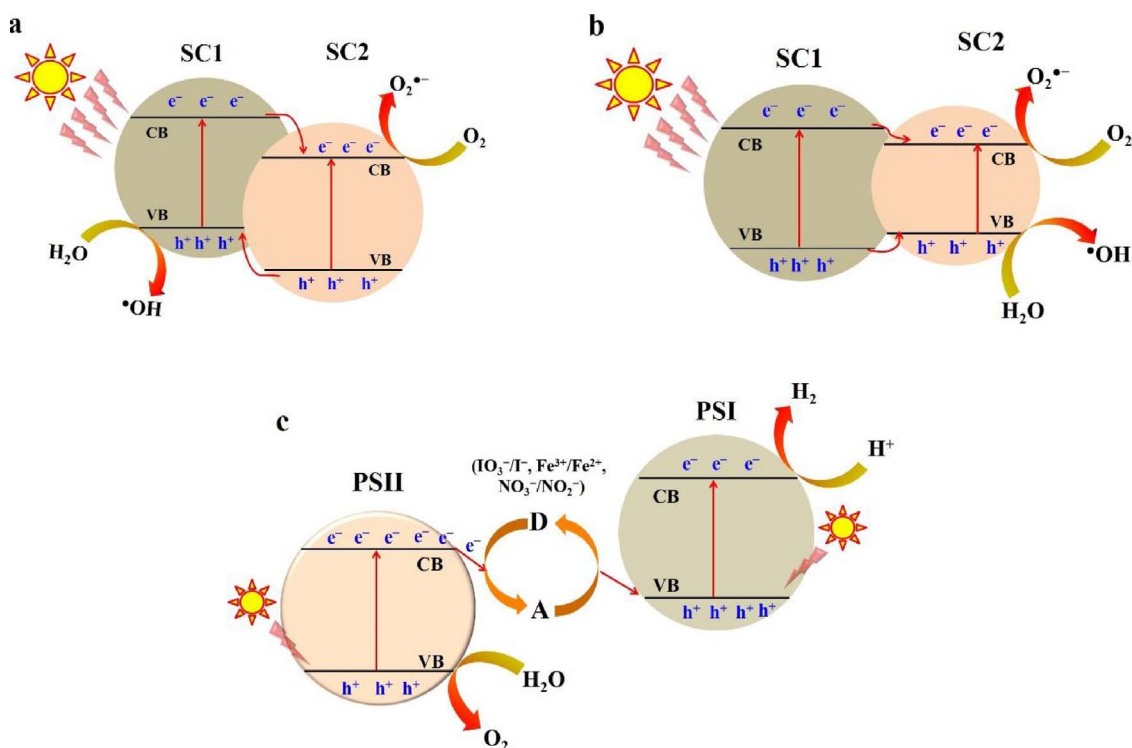
Fig. 2. Schematic representation of photogenerated electron-hole separation mechanism on (a and b) heterojunction-like photocatalysts and (c) Z-scheme type photosystem with shuttle redox-mediators.

and 2 remain effectively separated to improve the photocatalytic efficiency. Due to these advantages, different visible light active redox-mediator-free direct dual semiconductor systems have been reported for degrading pollutants. In our laboratory, we have synthesized g-C_3N_4, TiO_2, $CaIn_2S_4$, $ZnIn_2S_4$, Bi_2WO_6 and $BiVO_4$ based visible light responsive direct dual semiconductor photocatalytic systems for the degradation of dye and pharmaceutical pollutants. Subsequently, the separation mechanism of photogenerated electron hole pairs on these direct dual semiconductors and their influence in degradation efficiency have been investigated by different spectroscopic techniques and discussed in the forthcoming section.

2. Photocatalysis

Exposure of semiconductor photocatalysts to light irradiation with equal or greater than the band gap energy excites the VB electrons to its CB, leaving behind holes in the VB. Subsequently, holes in the VB travel to the surface and react with surface adsorbed water molecules (H_2O) or hydroxyl groups (-OH) to produce desired reactive ·OH radicals. Simultaneously, electrons in the CB move to the surface and react with dissolved oxygen (O_2) and generates superoxide radical anions ($O_2^{·-}$). These reactive radical species (·OH and $O_2^{·-}$) subsequently react with the pollutants, leading to intermediate products and finally mineralized into carbon dioxide, water and other inorganic ions. In some cases, the photogenerated holes directly oxidize the pollutants remaining adsorbed on the photocatalyst surface. In addition, the electrons indirectly degrade the pollutants using ·OH radicals produced through hydrogen peroxide (H_2O_2) decomposition, which is formed by the reaction of superoxide radical anions with protons (H^+). On the other hand, in dye degradation reaction the dye may be excited under light irradiation and inject an electron into the CB of the catalyst; they react with oxygen to yield hydroxyl (·OH) radicals indirectly via the formation of H_2O_2.

In 1976, Carry et al., used TiO_2 as a photocatalyst for photodechlorination of polychlorobiphenyls [13], followed by Frank and Bard, who utilized it for photocatalytic oxidation of cyanide and sulphite ions in water [14,15]. Subsequently, TiO_2 has been intensely used for

degradation of dyes, organic compounds, pharmaceuticals and metal ions reduction [13–23,64–68]. The band gap energy of TiO_2 has been tuned to absorb visible light, besides UV, by doping with metals (Ag, Au, Cu, Pt, Pd, Fe, Ni, Co, Mg, Zn, Bi, La etc.), non-metals (B, C, N, P, S, F), sensitized with dyes and made composites with other metal oxides [24–33,69–77]. As a result, the visible light response of TiO_2 improved and the photogenerated electrons are trapped by the dopant leading to better charge carrier separation and charge transfer resulting in enhanced reaction efficiencies. In addition, the surface area of TiO_2 was enhanced by changing the surface morphology and supporting it on high surface area solid adsorbent materials (zeolites, carbon, graphene, silica, and other meso and microporous materials). This also helped to enhance the adsorption of reactants onto the catalyst surface and thereby improve pollutant degradation efficiencies [78–82]. We have also worked on the TiO_2 and modified TiO_2 photocatalytic systems for the degradation of dyes and organic compounds [16,19,25,28,29,31,70,72]. However, the poor regeneration of modified catalyst and low reproducibility in degradation results are limiting their practical application. To overcome these constraints visible light responsive metal sulphides (eg. CdS, ZnS), tantalates, g-C_3N_4, bismuth (Bi_2O_3, Bi_2WO_6, $BiVO_4$, BiOX, Bi_2MoO_6 etc.), and ferrite etc., based photocatalysts have been prepared and studied. The metal sulphides in general show lower stability due to photocorrosion [34–38,83–86] and some of these faces even high rate of charge carrier recombination as well. To improve the photo-stability and charge carrier separation and charge transfer rate, heterojunction-like composites have been prepared by combining visible light responsive photocatalysts with other semiconductor catalysts. The heterojunction photocatalysts are thus defined as band-aligned materials with an interface between the two different semiconductors having unequal band structures. Typically, these are classified into two types. In type 1, the CB and VB levels of semiconductor 1 (SC1) is higher than the CB and VB levels of semiconductor 2 (SC2). Therefore, the photogenerated electrons on the CB of SC1 will transfer to CB of SC2. Simultaneously, the photogenerated holes on the VB of SC2 will transfer to VB of SC1 (Fig. 2a). The accumulated electrons and holes on the CB and VB of the SC2 and SC1 actively
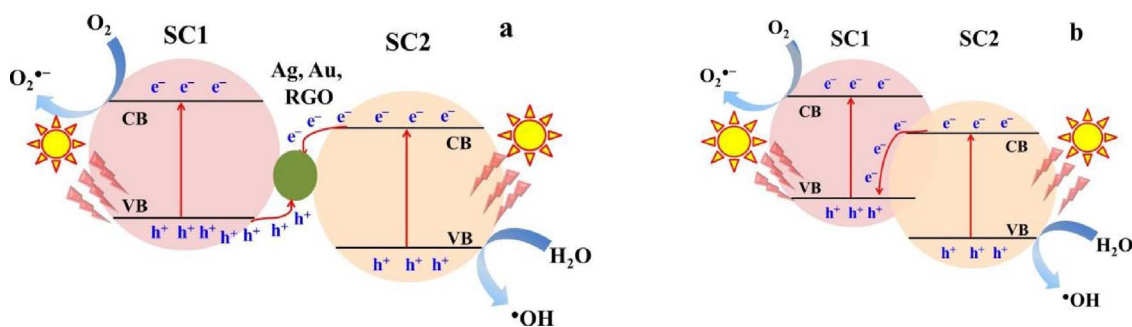
Fig. 3. Schematic representation of charge carrier separation mechanisms on dual semiconductor photocatalytic systems with (a) solid-sate electron mediators and (b) without redox-mediators (mediator free direct dual semiconductor systems).

participate in degradation reactions of species adsorbed on the surface. In type 2, the respective CB and VB levels of SC1 are higher and lower than the CB and VB levels of SC2. Thus, the photogenerated charge carrier transfer takes place as shown in Fig. 2b and the electrons and holes get accumulated at the CB and the VB levels of SC2. These accumulated charge carriers have lower redox potentials required for reactive radicals generation, thereby declining the photocatalytic activity of type 2 heterojunction photocatalyst (Fig. 2b) [87,88]. Ge et al., prepared g-C_3N_4/Bi_2WO_6 heterojunction-like photocatalyst, which showed a complete degradation of methyl orange (MO) dye when compared to the pristine Bi_2WO_6 (14.2%) under visible light irradiation [44]. Ye et al., studied the visible light activity of BiOBr/g-C_3N_4 for rhodamine B (RhB) dye degradation, which exhibited respectively 6.3 and 2.71 times higher activity than single g-C_3N_4 and BiOBr within 30 min of reaction [46]. Recently, Feng et al., revealed that CdS/Bi_2MoO_6 heterojunction photocatalyst displayed improved visible light degradation efficiency (88.7%) in RhB degradation when compared to pure Bi_2MoO_6 (2.0%) and CdS (22.3%), respectively [47]. Similarly, different visible light responsive heterojunction-like photocatalysts have been designed and studied [32,39–47]. Though the photogenerated charge carriers are efficiently separated in these photocatalysts, the position of VB (g-C_3N_4, +1.575 eV; CdS, +1.68 eV) where the holes are accumulated is lower than the ·OH radicals generation potential required, so these holes are not able to oxidize the H_2O to yield ·OH radicals. The accumulated holes may involve in the direct decomposition of pollutants; however, that pathway alone cannot mineralise pollutants completely. The redox ability of spatially separated charge carriers on this type of photocatalysts are insufficient, and further development of visible light driven dual semiconductor systems with or without redox-mediators are therefore required for effectively degrading pollutants in water.

3. Z-scheme photosynthesis with redox-mediators

In natural photosynthesis, sunlight serves as the energy source to produce O_2 and storable chemical energy, using CO_2 and H_2O. This process involves two photosystems, namely PS II and PS I, and is referred to as the 'Z-scheme' due to the electron excitation and energy transfer pathways. To mimic this process, artificial Z-scheme photosystems consisting of two semiconductors and shuttle redox-mediators have been developed to photoelectrochemically split water to produce O_2 and clean fuel H_2. Such Z-scheme semiconductor systems improve the visible light absorption and charge transfer rate of reactions leading to enhanced energy conversion (Fig. 2c). In 1979, Bard has introduced this Z-scheme concept for water splitting applications [48] with the H_2 and O_2 evolution process taking place in two different semiconductors aided by suitable shuttling redox couples (IO_3^-/I^-, Fe^{3+}/Fe^{2+}, NO_3^-/NO_2^-, for example.). Similarly, different Z-scheme photocatalysts consisting of Pt/TiO_2 anatase/TiO_2 rutile (IO_3^-/I^-), Pt/$SrTiO_3$:Rh/ $BiVO_4$ (Fe^{3+}/Fe^{2+}), Pt/$SrTiO_3$:Rh-Ru/$SrTiO_3$:In/V (IO_3^-/I^-), etc., have been also developed and reported [49–55]. However, the energy

conversion efficiencies of these photosystems are very low due to the poor stability of redox-mediators, high visible light absorption by the redox-mediators themselves and the backward reactions occurring between the products. To solve these difficulties, Z-scheme photosystems with solid electron mediators (metals, carbon and graphene) and redox-mediator-free direct Z-scheme photosystem have been developed, further [89–93]. To mimic these methods for effecting photocatalytic pollutant degradation reactions, recently catalyst systems looking like 'Z-schemes' with or without solid-state electron mediators have been developed. However, as described in Section 1, the Z-scheme denotes only thermodynamically uphill reactions ($\Delta G > 0$, Fig. 1a), and the photocatalytic degradation of pollutants are always thermodynamically downhill reactions ($\Delta G < 0$, Fig. 1b) and calling them Z-scheme photocatalysis should be avoided.

4. Dual semiconductor photocatalytic system with solid-state electron mediators

In this system, the photogenerated charge carriers are separated and transferred through solid electron mediators (metal nanoparticles (Ag, Au, Cu), RGO and carbon, for example) present at the interface of the two semiconductors. The charge carriers are expected to be efficiently separated between two semiconductors to enhance the catalytic efficiency (Fig. 3a). The various dual semiconductor photocatalytic systems with different solid-state electron mediators currently used for the degradation of pollutants under visible light irradiation are summarized and documented in Table 1 [94–136].

In 2006, Tada et al., developed a visible light driven solid-state CdS/Au/TiO_2 dual semiconductor photocatalytic system for methylviologen (MV^{2+}) reduction, which revealed that electron–hole pairs were efficiently separated through a vectorial electron transfer ($TiO_2 \rightarrow Au \rightarrow$ CdS), resulting in higher degradation efficiencies than the corresponding mono- and bi- photocatalytic systems. The vectorial electron transfer to the CB of TiO_2 continues to Au and then to the VB of the CdS where they recombine with the holes present on the VB. The electrons and holes on the CB and VB of the CdS and TiO_2 thus possess higher reduction and oxidation capabilities (Fig. 4) [56]. Similar vectorial electron transfer ($TiO_2 \rightarrow Au \rightarrow$ CdS) was observed by Zhu et al., in CdS/Au/TiO_2 hollow nanorod array (HNA) systems for MB dye degradation. The degradation results revealed that CdS/Au/TiO_2 HNAs improved the overall degradation efficiency (72%) from the bare THNAs (15%), Au-THNAs (35%) and CdS-THNAs (25%) systems [94]. Hu et al., synthesised Ag based (Ag/AgBr/TiO_2) system for the degradation of a variety of azo-dyes and *Escherichia coli* bacteria. They observed that AgBr is the only component active under visible light. However, the presence of Ag^0 species on the surface of the catalyst is responsible for improving the lifetime of electron-hole pairs and their interfacial charge transfer, which generates higher concentration of ·OH and O_2·$^-$ leading to higher degradation efficiencies [57]. Zhang et al., reported a AgBr-Ag-Bi_2WO_6 nanojunction system and demonstrated that both AgBr and Bi_2WO_6 generate electron-hole pairs under

Table 1

Dual semiconductor photocatalytic system with solid-state electron mediators (M) for degradation of pollutants under visible light irradiation.

SC1	SC 2	M	Light source (Power, W)	Pollutants	Concentration (mg/L): Volume (mL)	Degradation (%) and Time	Refs.
AgBr	Bi_2WO_6	Ag	Xe lamp (300)	MX-5B, PCP	50 (MX-5B), 10 (PCP): 100, 50	82 (MX-5B), ~ 63 (PCP) and 1 h	[58]
CdS	TiO_2 HNA	Au	LP Hg lamp (20)	MB	10:60	72 and 2 h	[94]
AgI	AgBr	Ag	Visible light (λ > 420 nm)	MO	3×10^{-5} M: 50	97 and 16 min	[95]
AgI	Ag_3PO_4	Ag	Xe lamp (500)	MO and PhOH	20 and 50	96.9 (MO), ~ 90 (PhOH) and 18 min	[96]
AgBr	MoO_3	Ag	Xe lamp (300)	RhB	NA:50	97.7 and 15 min	[97]
AgBr	Ag_3PO_4	Ag	Xe lamp (500)	AO 7	20:30	91.8 and 15 min	[98]
GO	AgCl	Ag	LED lamp ($\lambda \geq$ 420 nm)	MB	2.5×10^{-5} M: 50	100 and 1 h	[99]
$g-C_3N_4$	AgBr	Ag	Xe lamp (300)	RhB and MO	10:100	95 (RhB, MO) and 10 min	[100]
$g-C_3N_4$	Ag_2CO_3	Ag	Xe lamp (300)	RhB	5:100	100 and 40 min	[101]
$S-g-C_3N_4$	CdS	Au	Xe lamp (300)	RhB, MO, MB	10:100	100 (RhB, MO, MB) and 5 min (RhB), 10 (MO, MB) min	[102]
AgBr	$Bi_{20}TiO_{32}$	Ag	Xe lamp (500)	IPN	15:40	93.2 and 54 h	[103]
SiC	Ag_3PO_4	Ag	Xe lamp (300)	MO and PhOH	10:100	100 (MO,PhOH), and 25, 30 min	[104]
Ag_3PO_4	WO_{3-x}	Ag	Xe arc lamp (300)	RhB, MO, MB	10:100	100 (RhB), 100(MB), 100(MO) and 3, 2, 20 min	[105]
AgBr	Ag_2CO_3	Ag	Xe lamp (500)	RhB, MO	20:20	100 (RhB, MO) and 30 min	[106]
Cu_2O	$BiPO_4$	Au	Xe lamp (300)	MO	10:20	100 and 1 h	[107]
AgI	Bi_2MoO_6	Ag	Xe lamp (300)	RhB	20:100	93.6 and 15 min	[108]
Ag_2O	$BiVO_4$	Ag	Xe lamp (300)	RhB, MB RhB + MB	10 (RhB), 20 (MB), 5 + 10 (RhB +MB), 10 + 20 (RhB + MB): 50	100 (RhB), 100(MB), 100 (RhB + MB) and 15, 48, 20, 48 min	[109]
$g-C_3N_4$	Bi_2WO_6	RGO	Xe lamp (500)	TCP	20:250	98 and 2 h	[110]
Bi_2O_3	$BiVO_4$	RGO	Xe lamp (300)	Toluene	25 ppm	95.6 and 7 h	[111]
$g-C_3N_4$	BiOBr	Au	Xe lamp (300)	RhB	10:100	100 and 80 min	[112]
$g-C_3N_4$	$BiPO_4$	Au	Xe lamp (300)	MO	10: NA	88 and 160 min	[113]
MoS_2	Ag_3PO_4	Ag	Solar Xe arc lamp (35)	MB, RhB, MO and PhOH	20 (MB, RhB), 10 (MO), 5 (PhOH):30	100 (MB, RhB, MO), 95 (PhOH) and 1 h (MB), 80 min (RhB) 2 h (MO, PhOH)	[114]
$g-C_3N_4$	CdS	Au	Xe lamp (300)	RhB	10:100	100 and 20 min	[115]
$g-C_3N_4$	$BiVO_4$	NGQDS	Xe lamp (250)	TC, CIP, OTC	10:100	91.5 (TC), 72.4 (CIP), 66.7 (OTC) and 0.5, 2 h	[116]
$g-C_3N_4$	WO_3	Cu, Ag, Au	Xe arc lamp (500)	4-NPhOH	1×10^{-4} M: 25	100 and 2 h	[117]
Ag_3PO_4	$BiVO_4$	Ag/RGO	Xe lamp (300)	TC	10:100	95.67 and 1 h	[118]
$g-C_3N_4$	Bi_2MoO_6	RGO	Xe lamp (500)	RhB	10:250	97.3 and 1 h	[119]
$g-C_3N_4$	Ag_3PO_4	Ag	Xe lamp (300)	SMX	1:100	100 and 1.5 h	[120]
Cu_2O	AgBr	Cu	Xe arc lamp (300)	MO	7:50	98 and 50 min	[121]
$CuBi_2O_4$	Ag_3PO_4	Ag	Xe lamp (300)	TC	10:100	75 and 1 h	[122]
$g-C_3N_4$	TiO_2	RGO	Xe lamp (300)	MB	30:200	92 and 3 h	[123]
In_2S_3	Ag_2CrO_4	Ag	Xe arc lamp (300)	MO	10:150	65.3 and 3 h	[124]
CdS	$BiVO_4$	Au	Xe lamp (300)	RhB and TC	10:50	100 (RhB), 91 (TC) and 90 min	[125]
CdS	Bi_2MoO_6	Ag	Halogen lamp (400)	RhB	10:200	100 and 80 min	[126]
$ZnS(en)_{0.5}$	Ag_3PO_4	Ag	Xe lamp (350)	MB and PhOH	20:20	82 and 160 min	[127]
$g-C_3N_4$	Bi_2MoO_6	CNT	Xe lamp (500)	2,4-DBP	20:250	68.8 and 2 h	[128]
3DOM-$SrTiO_3$	Ag_3PO_4	Ag	Xe lamp (300)	RhB, MB and PhOH	10:50 (RhB, PhOH) 20:50 (MB)	100 and 12 min (RhB, MB), 100 and 16 min (PhOH)	[129]
TiO_2	WO_3	RGO	Arc Hg-Xe lamp (200)	E. coli	NA	97.3 ± 3.8% and 80 min	[130]
CdS	BiOCl	Au	Xe lamp (300)	MO, RhB, PhOH, and SD	20:50 (MO, RhB, SD) 10:50 (PhOH)	100 and 3 h (MO), 100 and 30 min (RhB), 100 and 100 min (PhOH), 100 and 4 h (SD)	[131]
$g-C_3N_4$	Ag_2CrO_4	Ag	HP Xe lamp (500W)	2,4-DCP	10:50	94 and 2 h	[132]
AgCl	$AgFeO_2$	Ag	Xe lamp (300)	RhB	10:100	100 and 1 h	[133]
CdS	WO_3	CDts	Xe lamp (150)	4CP, RhB, TCH and Cr(VI)	20:100 (4CP, RhB), 30:100 (TCH), 10:100 (Cr(VI))	70 and 7 h (4CP), ~ 96.1 and 70 min (RhB), 98.7 and 3 h (TCH), 94.6 and 2 h (Cr(VI))	[134]
$ZnFe_2O_4$	AgBr	Ag	Xe lamp (300)	E. coli and MO	$10^{5.5}$ cfu/mL (E. coli), 10:70 (MO)	100:2 h (E. coli), 93.20 and 6 min (MO)	[135]
Ag_2CO_3	WO_3	Ag	Xe lamp (300)	RhB, MO, CIP, TC	20:100 (RhB), 10:100 (MO, CIP, TC)	99.13 and 1h (RhB), 86.1 (MO), 83.9 (CIP), 81.4 (TC) and 1.5 h	[136]

* NA − Data not available.

visible light, which were separated by the flow of electrons on the CB of Bi_2WO_6 to metal Ag because of the relative position CB of Bi_2WO_6 *vs* Ag. Simultaneously, the holes on the VB of AgBr flow into metal Ag. Thus, the electrons and holes on the CB and VB of AgBr and Bi_2WO_6 hold strong redox capability for degradation of procion Red MX–5 B and pentachlorophenol pollutants [58]. Similarly, Iwase et al., used reduced graphene oxide (RGO) as an electron mediator in the $BiVO_4$/Ru/$SrTiO_3$:Rh Z-scheme photosystem for water splitting, which revealed that RGO can shuttle the electrons between the $BiVO_4$ and Ru/$SrTiO_3$: Rh and increases the consumption of electron-hole pairs in water splitting reactions under visible-light irradiation [137]. RGO possesses a high electrical conductivity that facilitates the transfer of charge carriers together with a large specific surface area to adsorb higher amounts of pollutants. Shi et al., developed $BiVO_4$/RGO/Bi_2O_3 solid

state dual semiconductor photocatalytic systems for the degradation of indoor air pollutant, toluene, under visible light irradiation. Visible light absorption by photocatalyst is enhanced by the RGO presence with improved separation of charge carriers by virtue of flow of elections from the higher to the lower Fermi levels in order to attain the thermodynamic equilibrium. The electrons on the CB of n-type $BiVO_4$ travels to p-type VB of Bi_2O_3 through the RGO mediator, where it recombines with holes. Thus, the electrons and holes on the CB and VB of the Bi_2O_3 and $BiVO_4$ were efficiently separated, leading to the enhanced toluene degradation efficiency (95.6%) [111]. Yan et al. prepared nitrogen-doped graphene quantum dots (NGQDs)-$BiVO_4$/$g-C_3N_4$ for the degradation of tetracycline (TC), oxytetracycline (OTC) and ciprofloxacin (CP) antibiotics in water. Charge carriers are efficiently separated through NGQDS under visible light irradiation (Fig. 5): 5%
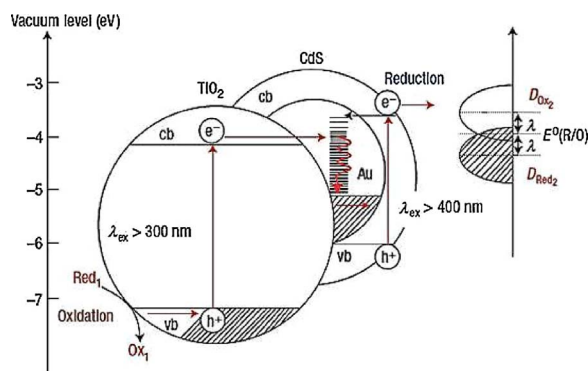
Fig. 4. Energy band diagram and charge carrier separation mechanism on CdS/Au/TiO$_2$. Reprinted with permission from Ref. [56].
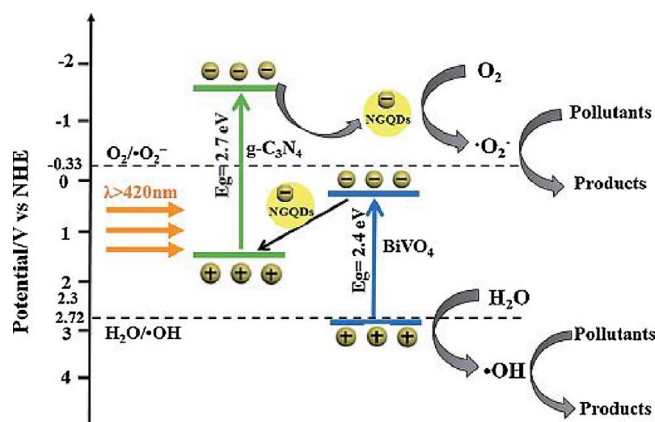

Fig. 5. Schematic representation of charge carrier separation and migration on 5% NGQDs-BiVO$_4$/g-C$_3$N$_4$ (1:2) photocatalyst. Reprinted with permission from Ref. [116].

NGQDs-BiVO$_4$/g-C$_3$N$_4$ (1:2) system degraded 91.5% of TC in 30 min as compared to BiVO$_4$/g-C$_3$N$_4$ (1:2, 72.3%), BiVO$_4$ (31.3%) and g-C$_3$N$_4$ (10.2%), respectively. Similarly, 72.4% CIP and 66.7% OT were degraded in 120 min using 5%NGQDs-BiVO$_4$/g-C$_3$N$_4$ (1:2) photocatalyst [116]. Ma et al. synthesized g-C$_3$N$_4$/RGO/Bi$_2$MoO$_6$ system for RhB dye degradation; demonstrated that matched Fermi level structure of g-C$_3$N$_4$ and Bi$_2$MoO$_6$ favours the interfacial charge transfer through RGO mediator resulting in the degradation of 97.3% of RhB dye within 60 min. This is 8.73 times higher activity than the pure Bi$_2$MoO$_6$ [119]. Recently, Zeng et al., prepared TiO$_2$ and WO$_3$ based dual semiconductor systems with RGO as a mediator for inactivation of gram-negative bacteria *Escherichia coli* under visible light irradiation. TiO$_2$/RGO/WO$_3$ showed significant *E. coli* inactivation efficiency (97.3 ± 3.8%) within 80 min compared to TiO$_2$/WO$_3$ (78.9 ± 2.6%) and WO$_3$/RGO (45.5 ± 3.7%) systems [130]. Different dual semiconductor photocatalytic systems with electron mediator such as AgI/Ag/AgBr, Ag@AgBr/g-C$_3$N$_4$, sulfur-doped g-C$_3$N$_4$/Au/CdS, Ag$_3$PO$_4$/Ag/SiC, Ag$_3$PO$_4$/Ag/WO$_{3-x}$, Ag$_2$CO$_3$/Ag/AgBr, AgI/Ag/Bi$_2$MoO$_6$, g-C$_3$N$_4$/Au/BiPO$_4$, CdS/Au/g-C$_3$N$_4$, WO$_3$-metal-gC$_3$N$_4$ (Metal = Cu, Ag, Au), Cu$_2$O/Cu/AgBr/Ag, g-C$_3$N$_4$/RGO/Bi$_2$WO$_6$, and RGO-Ag$_3$PO$_4$/Ag/BiVO$_4$ etc., have been developed for the degradation of different dyes and organic compounds [94–136]. However, these systems hold drawbacks such as visible light reaching the surface of catalyst was reduced by electron mediators (metal) present due to surface plasmon resonance effect. Besides, the nanocarbon and graphene synthesis involves intricate procedures of high energy consumption. Therefore, redox-mediator-free direct dual semiconductor photocatalytic systems have been developed to circumvent such drawbacks.

5. Direct dual semiconductor photocatalytic system (without redox-mediators)

A direct dual semiconductor photocatalytic system is defined as one involving an interface between two semiconductors (SC1 and SC2) by joining them together without the need of redox-mediators or electron mediators. The photogenerated electron-hole-pair separation mechanism follows the inter cross sectional electron transfer, which is different to the charge separation mechanism seen in the previously described heterojunction-like composites. Under visible light irradiation electron-hole pairs are generated on both the semiconductors (SC1 and SC2), then the inter cross sectional electron transfer occurs via the travel of electrons on the CB of SC2 to VB of SC1 where they combine with the holes. Subsequently, the presence of electrons on the CB of SC1 and holes on the VB of SC2 are well separated and possess higher redox potential than the O$_2$· − (−0.33 eV vs. NHE) and ·OH (+2.4 eV vs. NHE) radical's production potentials (Fig. 3b). This electron-hole pair transfer mode eliminates the photon shielding problem caused by the presence of redox mediators, leading to higher visible light absorption by the semiconductor photocatalysts. In 2007, Arai et al., developed CuBi$_2$O$_4$/WO$_3$ direct dual semiconductors by mechanical mixing for the degradation of acetaldehyde (CH$_3$CHO). The results revealed that the photogenerated electrons and holes on the CB of n-type WO$_3$ and VB of p-type CuBi$_2$O$_4$ recombine. Thus, the holes in WO$_3$ and electrons in CuBi$_2$O$_4$ exhibit strong oxidation and reduction potentials, which helps to degrade the CH$_3$CHO within 60 min rather than with the case of using solely WO$_3$ (180 min) and CuBi$_2$O$_4$ (180 min,). The rate of CO$_2$ regeneration is also higher as compared to using WO$_3$, CuBi$_2$O$_4$ and TiO$_2$, solely (Fig. 6) [60]. Subsequently, they synthesized CuO/WO$_3$
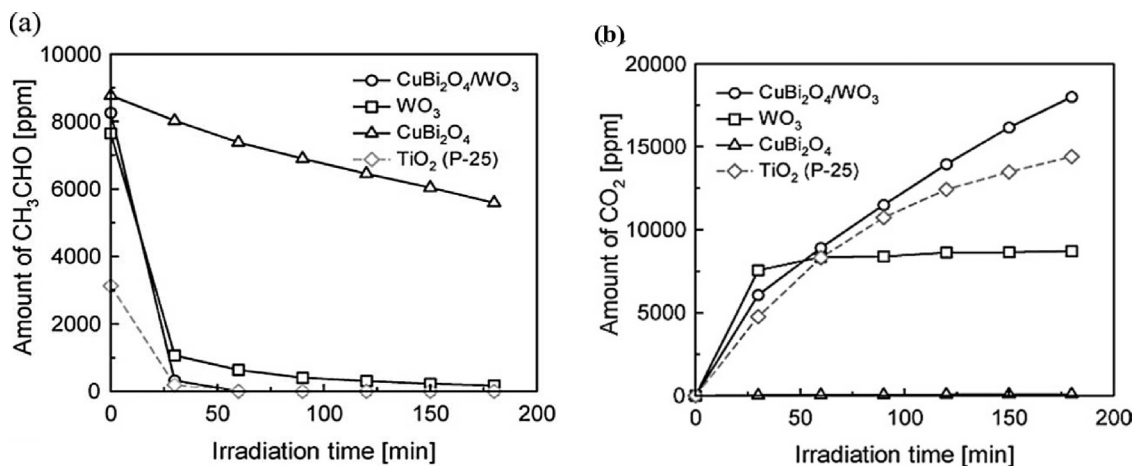

Fig. 6. (a) Degradation of CH$_3$CHO and (b) generation of CO$_2$ during the reaction using CuBi$_2$O$_4$/WO$_3$ under visible light irradiation. Reprinted with permission from Ref. [60].
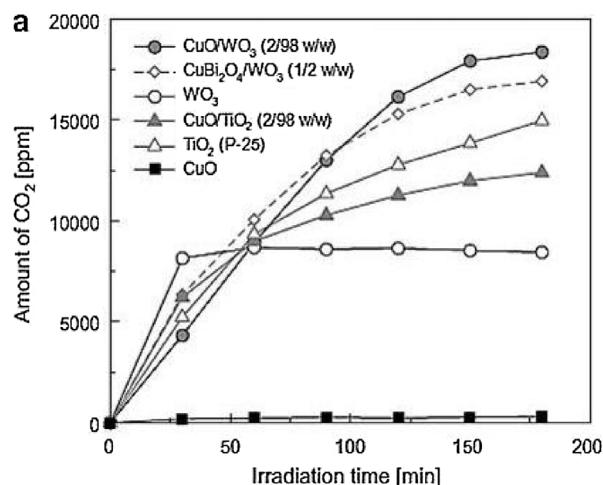
Fig. 7. Time profile of (a) CO_2 generation and (b) CH_3CHO decomposition during the degradation reaction of CH_3CHO over CuO/WO_3 photocatalyst under visible light irradiation. Reprinted with permission from Ref. [138].
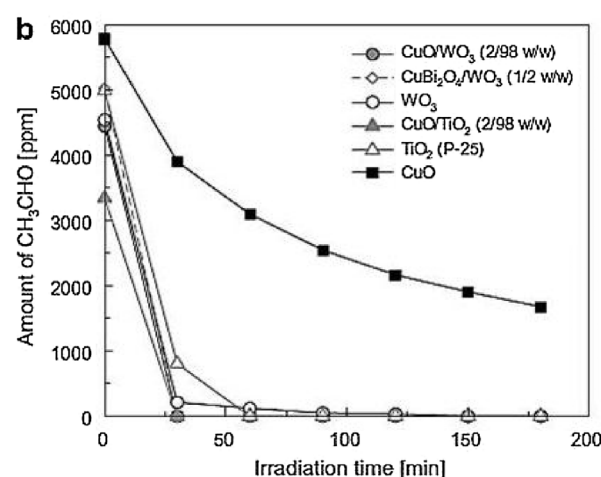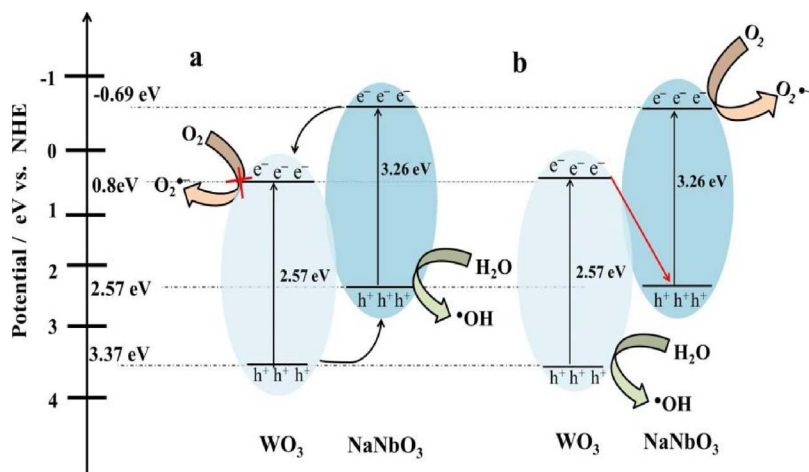

Fig. 8. Charge carrier separation mechanism on $NaNbO_3/WO_3$ system (a) heterojunction-like and (b) inter cross sectional electron transfer. Reprinted with permission from Ref. [61].

system and investigated their catalytic efficiency for the degradation of CH_3CHO under xenon or white fluorescent lamp irradiation. CuO/WO_3 system follows the same mechanism as $CuBi_2O_4/WO_3$ system in separation and migration of electron-hole pairs, leading to complete oxidization of CH_3CHO. The catalytic performance is compared to WO_3, CuO, TiO_2, CuO/TiO_2 and $CuBi_2O_4/WO_3$ (Fig. 7). Both the $CuBi_2O_4/WO_3$ and CuO/WO_3 system showed almost the same degradation efficiency, however CuO/WO_3 exhibited slightly higher activity than the $CuBi_2O_4/WO_3$. This may be due to the difference in the photoelectrochemical behaviour of unstable CuO compared to relatively more stable $CuBi_2O_4$. The catalytic effectiveness of CuO/WO_3 system when compared to WO_3 and CuO, is also seen with volatile organic compounds (VOCs) such as small aldehyde, acid, ether and hydrocarbon molecules [138,139]. Shifu et al., designed $NaNbO_3/WO_3$ system for RhB, MB degradation and Cr^{6+} reduction. $NaNbO_3$ (0.5 wt%)/WO_3 showed 3–5 times higher photocatalytic activity for degradation of dyes than the pure WO_3. Similarly, Cr^{6+} was reduced more effectively when using $NaNbO_3$ (0.5 wt%)/WO_3 than pure WO_3. If the charge carrier transfer follows the conventional heterojunction type separation mechanism (Fig. 8a), the accumulated electrons on the CB of WO_3 (+0.8 eV vs NHE) and holes on the VB of $NaNbO_3$ (+2.57 eV vs NHE) become less effective in the production of $O_2 \cdot -$ and $\cdot OH$ radicals. However, quenching of reactive radicals by different scavengers and hydroxyl radicals determined by fluorescence spectroscopy analysis, demonstrated that $\cdot OH$ and $O_2 \cdot^-$ radicals actively participate in the degradation reaction. Therefore, the charge carriers in $NaNbO_3/WO_3$

system were efficiently separated via the inter cross sectional electron transfer mechanism. In this mechanism, the electrons on the CB of WO_3 travels to the VB of $NaNbO_3$ and recombine quickly with the holes on its VB. Eventually, the electrons on the CB of $NaNbO_3$ (-0.69 eV vs NHE) and holes on the VB of the WO_3 (3.37 eV vs. NHE) were efficiently separated (Fig. 8b) as evidenced by electron spin resonance (ESR) and photoluminescence spectroscopy analysis [61]. $Bi_2O_3/NaNbO_3$ system similarly revealed that the heterogeneous junctions are better photocatalysts than the bare Bi_2O_3 and $NaNbO_3$ [140].

Recently, $g-C_3N_4$ has received greater attention for absorption of higher amount of visible light due to its lower band gap (2.7 eV). Its layered structure provides high surface area and electrons are on a highly negative CB edge level (-1.135 eV vs. NHE) leading to a strong reduction potential. Nevertheless, the rapid recombination of charge carriers over $g-C_3N_4$ lowers the degradation efficiency [35,141,142] and it could be overwhelmed by combining them with other semiconductors having adequately high positive VB levels to form direct dual semiconductor photocatalysts. A list of different representative redox-mediator-free dual semiconductor photocatalytic systems used for degradation of pollutants are provided in Table 2 [143–205]. Yu et al., developed $g-C_3N_4/TiO_2$ direct dual semiconductors for the degradation of formaldehyde (HCHO). The holes in the TiO_2 remain on the VB of TiO_2, whereas the electrons on the CB of TiO_2 travel to the VB of $g-C_3N_4$, where they combine with the holes on the VB of $g-C_3N_4$. Consequently, the holes and electrons on the VB and CB of TiO_2 and $g-C_3N_4$ gets efficiently separated, with sufficient positive and negative

Table 2
Redox-mediator-free direct dual semiconductor photocatalytic system for degradation of pollutants under visible light irradiation.

SC1	SC2	Light source (power, W)	Pollutants	Concentration (mg/L): Volume (mL)	Degradation (%) and Time	Refs.
CaFe$_2$O$_4$	WO$_3$	Xe lamp (150)	CH$_3$CHO	100 ppm: NA	100 and 15 h	[59]
CuBi$_2$O$_4$	WO$_3$	Xe lamp (300)	CH$_3$CHO	9000 ppm: NA	100 and 3 h	[60]
NaNbO$_3$	WO$_3$	MP Hg lamp (375)	MB, RhB and Cr (VI)	1×10^{-5} mol/L (RhB), 5×10^{-5} mol/L (MB), 3×10^{-5} mol/L (Cr)	90 (MB), 96 (RhB), 62.6 (Cr^{6+}) and 80, 25 and 40 min	[61]
g-C$_3$N$_4$	TiO$_2$	UV lamp (15)	HCHO	170 $\pm$ 10 ppm: NA	94 and 1 h	[62]
NaNbO$_3$	Bi$_2$O$_3$	MP Hg lamp (375)	RhB, MB	1×10^{-5} (RhB), 1×10^{-5} (MB) mol/L:300	91, 87 and 40, 15 min	[140]
g-C$_3$N$_4$	WO$_3$	Xe lamp (500)	MB, BF	0.9×10^{-5} (MB) and 1×10^{-5} (BF) mol/L	87.9 (MB), 75.6 (BF) and 1 h	[143]
g-C$_3$N$_4$	N-ZnO	Xe lamp (300)	RhB	5:100	100 and 1 h	[144]
g-C$_3$N$_4$	Ag$_3$PO$_4$	Xe lamp (300)	Ethylene	90 µl: NA	100 and 3 h	[145]
g-C$_3$N$_4$	Bi$_2$O$_3$	Xe lamp (500)	MB, RhB	1.1×10^{-5} (MB), 1×10^{-5} (RhB) mol/L and 300	78.1 (MB), 45.6 (RhB) and 1 h	[146]
g-C$_3$N$_4$	BiOCl	Xe lamp (300)	RhB	10:200	99 and 1 h	[147]
g-C$_3$N$_4$	MoO$_3$	Xe lamp (350)	MO	100:100	NA	[148]
Cu$_2$O	NaTaO$_3$	Hg lamp (300)	RhB	2×10^{-5} M:50	100 and 3 h	[149]
GO	Ag$_2$CrO$_4$	Xe arc lamp (500)	MB, RhB, MO, PhOH	1×10^{-5} mol/L (MB, RhB, MO), 10 (PhOH):100	100 (MB, RhB, MO), 90 (PhOH) and 15, 28, 40, 60 min	[150]
AgI	β-Bi$_2$O$_3$	Tungsten lamp (500)	MO, TC	10:60, 7.3 mol/L:30	97.8, 80 and 4, 2 h	[151]
g-C$_3$N$_4$	Ti^{3+}-TNTA	Visible light (λ > 420 nm)	PhOH	10:50	74 and 7 h	[152]
MoS$_2$	TiO$_2$@Zeolite	Xe arc lamp (500)	MO	20:250	95 and 1 h	[153]
PbWO$_4$	WO$_3$.0.33H$_2$O	Xe lamp (300)	RhB, MO	10:100	100, 82 and 1 h	[154]
g-C$_3$N$_4$	TiO$_2$	Hg lamp (200)	ISN	50:500	79.5 (CN-TNP), 90.8 (CN/TNT) and 4 h	[155]
g-C$_3$N$_4$	BiVO$_4$	Xe lamp (500)	RhB	1×10^{-5} mol/L:50	85 and 5 h	[156]
g-C$_3$N$_4$	Bi$_2$MoO$_6$	LED (50, 400 nm)	MB	10:30	90 and 40 min	[157]
g-C$_3$N$_4$	Bi$_2$WO$_6$ QD	Xe lamp (500)	RhB	10:50	100 and 40 min	[158]
CdWO$_4$	WO$_3$	Xe lamp (500)	MO, RhB, MB	10:100	95(MO), 95 (RhB), 97 (MB) and 50, 40, 50 min	[159]
CaIn$_2$S$_4$	TiO$_2$	Hg lamp (200)	MTZ, ISN	50:500	100 (MTZ), 71.9 (ISN) and 4 h	[160]
g-C$_3$N$_4$	Vo-ZnO	Xe lamp (300)	MO, HA	10:50	93 (MO), 80(HA) and 1, 1 h	[161]
g-C$_3$N$_4$	Ag$_3$PO$_4$	Xe-arc lamp (300)	MB	0.9×10^{-5} M:100	96.8 and 0.5 h	[162]
g-C$_3$N$_4$	WO$_3$	Xe lamp (500)	MB, BF	0.9×10^{-5} (MB) and 1×10^{-5} (BF) mol/L	87.9(MB), 75.6 (BF) and 1 h	[163]
RGO	Ag$_3$PO$_4$	Xe lamp (300)	RhB, Rh6G, MB, CR, MO	20:10	100, 76.26, 98.58, 69.88, 69.92 and 5 min	[164]
AgI	CeO$_2$	Xe lamp (150)	RhB	10:100	98.99 and 70 min	[165]
g-C$_3$N$_4$	V$_2$O$_5$	Xe lamp (250)	MB, MO, RhB, TC	10:100	100 (MB), 100 (MO), 95.5 (RhB), 75.5 (TC) and 2, 2, 1, 2 h	[166]
ZnIn$_2$S$_4$	Bi$_2$WO$_6$	tungsten-halogen lamp (500)	MTZ	10:500	56 and 4 h	[167]
Bi$_2$MoO$_6$	Ag$_3$PO$_4$	LED (50, 410 nm)	MB	8:30	96.8 and 90 s	[168]
2D-g-C$_3$N$_4$ NS	2D-TiO$_2$ NS	Xe lamp (300)	MO	10:100	100 and 1 h	[169]
AgI	WO$_3$	Xe lamp (300)	TC	35:40	75 and 1 h	[170]
Ag$_4$V$_2$O$_7$	Ag$_3$VO$_4$	Xe lamp (400)	MB, PhOH	25, 40:30	100, 62.1 and 2.5, 5 h	[171]
g-C$_3$N$_4$	SnO$_{2-x}$	LED lamp (30)	RhB	10:80	100 and 100 min	[172]
g-C$_3$N$_4$	Ag$_2$CrO$_4$	Xe lamp (300)	RhB, MO	10:50	100 (RhB), 90 (MO) and 40, 21 min	[173]
g-C$_3$N$_4$	CoFe$_2$O$_4$	Xe lamp (500)	RhB	10: 100	100 and 3.5 h	[174]
g-C$_3$N$_4$	PI	Xe lamp (300)	NO	600 ppb	100 and 1 h	[175]
MoS$_2$	Ag$_3$PO$_4$	tungsten-halogen lamp (150)	RhB	20:100	100 and 16 min	[176]
CdS	BiOI	Xe lamp (300)	RhB	20:100	88.3 and 1.5 h	[177]
g-C$_3$N$_4$	TNTA	Xe lamp (300)	RhB	5:20	67 and 5 h	[178]
Ag$_3$PO$_4$	WO$_3$	Xe lamp (300)	MB, MO	10:100	95 (MB), 90 (MO) and 1, 3 h	[179]
g-C$_3$N$_4$ QD	Rutile TiO$_2$	Xe lamp (500)	RhB	5:50	100 and 4 h	[180]
g-C$_3$N$_4$	Ag$_2$WO$_4$	Xe lamp (300)	MO	10:30	95 and 2.5 h	[181]
g-C$_3$N$_4$	TiO$_2$	Xe lamp (300)	Propylene	600 ppm V:12 µl	56 and 8 h	[182]
MoS$_2$	Bi$_2$WO$_6$	Xe lamp (400)	RhB	10:40	100 and 4 h	[183]
Bi$_2$MoO$_6$	BiOBr	Xe lamp (300)	RhB, CIP	1×10^{-5} mol/L, 10 and 50	95 (RhB), 84.63 (CIP) and 10 min, 2 h	[184]
g-C$_3$N$_4$	WO$_3$	Xe lamp (500)	RhB	5:50	100 and 2 h	[185]
g-C$_3$N$_4$	Bi$_{12}$GeO$_{20}$	Day lamp (300)	RhB, mLR, Cr (VI)	5, 0.5 and 10: 100, 20, 100 (RhB, mLR, Cr (VI))	100 (RhB), 97 (mLR), 100 (Cr(VI) and 2.5 h, 50 min, 3 h	[186]
g-C$_3$N$_4$	Natural Laiwu hematite ore (LW)	Halogen lamp (300)	MB	4:250 and 30% H$_2$O$_2$ (25 µl)	97 and 1 h	[187]
g-C$_3$N$_4$	WO$_3$	Xe lamp (300)	MB	50:100	95 and 90 min	[188]
g-C$_3$N$_4$	Bi$_2$Sn$_2$O$_7$	Xe arc lamp (300)	MB and AR18	10:50	94.7 (MB), 93 (AR18) and 3 h	[189]
BiO$_{1-x}$Br	Bi$_2$O$_2$CO$_3$	Xe lamp (500)	CIP, BPA, 4-MAA	40 20, 50:40 (CIP, BPA, 4-MAA)	100 (CIP, BPA, 4-MAA) and 3 h	[190]
CdS	InVO$_4$	Xe lamp (250)	RhB and CIP	10:100	93.1 and 40 min	[191]
g-C$_3$N$_4$	WO$_3$	Xe arc lamp (300)	SMX	10:40	76.7 and 4 h	[192]

Table 2 (*continued*)

SC1	SC2	Light source (power, W)	Pollutants	Concentration (mg/L): Volume (mL)	Degradation (%) and Time	Refs.
mp-g-C_3N_4	Bi_2WO_6	Xe lamp (300)	TC and RhB	50:50 (TC), 20:50 (RhB)	100 and 1 h (RhB), 75 and 2 h (TC)	[193]
$KNbO_3$	Bi_2O_3	MP Hg lamp (375)	RhB and MO	3×10^{-6} mol/L (RhB), 1×10^{-5} mol/L (MO):150	92.2 (RhB), 90.8 (MO) and 30 min	[194]
SiC	Ag_2CO_3	Solar light	MB	78 µM:800	100:1.5 h	[195]
Py- g-C_3N_4	$BiVO_4$	Visible light	PhOH and MO	10:150	97.1 (PhOH), 92 (MO) and 2.5 h	[196]
PI	P-WO_3	Visible light	Imidacloprid	20:50	50 and 2.5 h	[197]
g-C_3N_4	Bi_4O_7	Halogen lamp (500)	MB, RhB, PhOH, BPA	5(MB), 4×10^{-4} M (PhOH), 1×10^{-5} M (RhB), 20 (BPA):80	100 and 1.5 h(MB), 93 and 140 min (PhOH), 100 and 70 min (RhB), 100 and 100 min (BPA)	[198]
$SnNb_2O_6$	WO_3	Tungsten lamp (500)	RhB	10:40	93.4 and 3 h	[199]
g-C_3N_4 NS	BiOBr NP	Xe lamp (300)	RhB and BPA	1×10^{-5} M:100(RhB), 5:100 (BPA)	100 and 50 min (RhB), 100 and100 min (BPA)	[200]
AgBr	MoO_3	Xe lamp (250)	RhB	10:200	95 and 5 min	[201]
g-C_3N_4 NS	MnO_2 NS	Xe lamp	RhB and PhOH	NA	91.3 and 1 h (RhB), 73.6 and 3 h (PhOH)	[202]
CdS	$Bi_4V_2O_{11}$	Visible light (250)	CIP, TC, RhB	10: 100	76.97 (CIP), 83.7 (TC), 95.7 (RhB) and 2 h	[203]
g- C_3N_4	$LaFeO_3$	LED (3)	MB	5:100	95 and 2 h	[204]
S-g- C_3N_4	Sm_2O_3	Visible light	MB	8:100	92.6 and 2.5 h	[205]

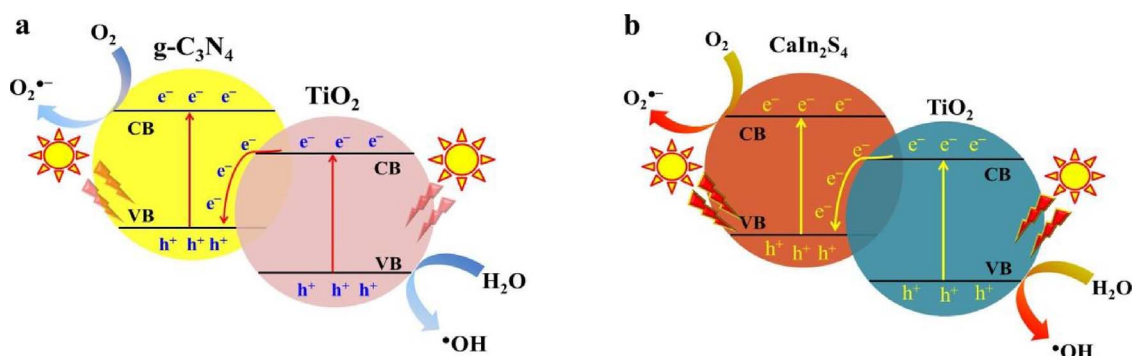*NA − Data not available.

Fig. 9. Representation of electron-hole transfer mechanism on (a) g-C_3N_4/TiO_2 and (b) $CaIn_2S_4$/TiO_2 direct dual semiconductors. Reprinted with permission from Refs. [155,160].
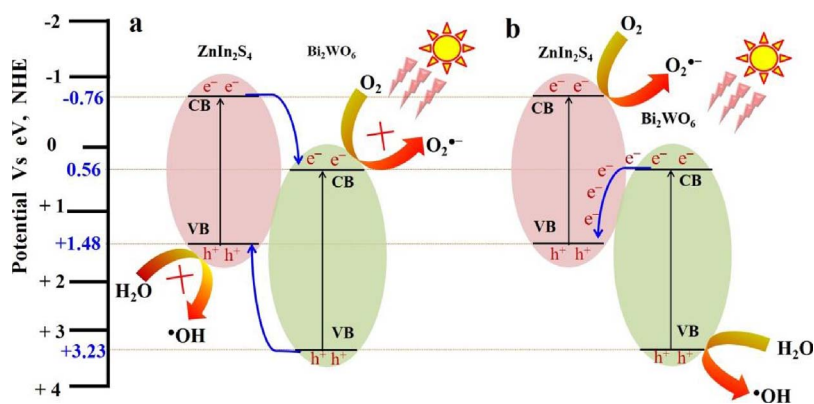

Fig. 10. Schematic representation of electron-hole separation mechanism on $ZnIn_2S_4$/Bi_2WO_6 (a) heterojunction-like and (b) inter cross sectional electron transport. Reprinted with permission from Ref. [167].

potentials for performing redox reactions: a fact proved by radicals quenching and ·OH radical determination by fluorescence spectroscopy studies [62]. g-C_3N_4/TiO_2 direct dual semiconductors have also been developed and the influence of TiO_2 morphology (nanoparticle and nanotube) on the catalytic performance was studied by degradation of isoniazid (ISN) pharmaceutical pollutants. The study demonstrated that 3%-g-C_3N_4/TiO_2 (nanotube) exhibited higher (90.8%) photocatalytic activity than the g-C_3N_4/TiO_2 (nanoparticle, 73.5%), TiO_2 nanotube (73.3%), TiO_2 nanoparticle (56.3%) and g-C_3N_4 (13.5%), respectively. The enhancement of the photocatalytic activity is due to the effective separation of the charge carriers between the g-C_3N_4 and TiO_2 through inter cross sectional electron transfer (Fig. 9a) [155]. Various g-C_3N_4

based direct dual semiconductor photocatalysts such as g-C_3N_4/WO_3, g-C_3N_4/Bi_2O_3, g-C_3N_4/BiOCl, g-C_3N_4/$BiVO_4$, g-C_3N_4/Bi_2WO_6, g-C_3N_4/Ag_2WO_4 etc., have been further developed (Table 2).

MoS_2 is another layered graphene-like material having high surface area and a number of reactive sites. It acts as an electron acceptor and increases visible-light absorption and charge carrier separation and transfer rate, which results in enhanced photocatalytic activity [83]. Similarly, silver orthophosphate (Ag_3PO_4) has received considerable attention due to its high photooxidative capabilities for organic pollutants under visible light irradiation [36]. However, the poor stability of the catalyst and the low reproducibility of degradation results warranted the development of direct dual semiconductor photocatalysts
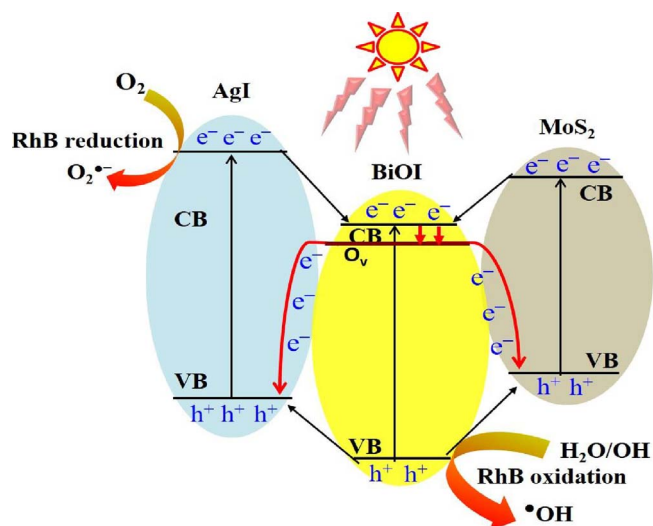
Fig. 11. Electron-hole separation mechanism on MoS$_2$/BiOI/AgI ternary photocatalytic system. Reprinted with permission from Ref. [213].

(Table 2). Chen et al., developed g-C$_3$N$_4$/Ag$_3$PO$_4$ direct dual semiconductor for the degradation of ethylene (C$_2$H$_4$) under visible light irradiation, and demonstrated that g-C$_3$N$_4$ improves the adsorption of gases and C$_2$H$_4$ gets completely degraded within 3 h when using g-C$_3$N$_4$/Ag$_3$PO$_4$ with a mass ratio of 7:3. The superior degradation activity is again attributed to the effective separation of electron-hole pairs via inter cross sectional electron transfer between the semiconductors, which has been proved by low intense photoluminescence

spectra of the g-C$_3$N$_4$/Ag$_3$PO$_4$ composites. The stability study revealed that photocatalyst was stable up to 5 cycles. Reactivation by heat-treatment at 450 °C for 3 h was effective for another five cycles of photocatalysis. It appears that the regeneration of nanosilver during heat treatment plays a vital role in the degradation ability of regenerated catalysts [145]. Xiong et al., improved the visible light response of (BiO)$_2$CO$_3$ by making direct dual semiconductor with MoS$_2$ ((BiO)$_2$CO$_3$/MoS$_2$) by doping. The lifetime of charge carriers improved by promoting their separation through inter cross sectional electron transport mechanism and showed that higher NO removal efficiency is possible via the new combination of semiconductors. The photocatalyst was stable up to only five catalytic cycles due to photo-corrosion of MoS$_2$ by holes (h$^+$) formed over (BiO)$_2$CO$_3$/MoS$_2$ [206].

In addition to g-C$_3$N$_4$, Ag$_3$PO$_4$ and MoS$_2$, ternary chalcogenide AB$_2$X$_4$ (A = Cu, Zn, Cd, Ca, etc.; B = In, Ga, Al; X = S, Se,) based visible-light responsive photocatalysts have also attracted attention due to their narrow band gaps, unique electronic and optical properties as well as excellent photo- and chemical stabilities. They were predominantly utilized for photo-production of H$_2$ from water [207,208]. Because of the stability of these systems it has been also used for designing composites and direct dual semiconductor photocatalysts for both H$_2$ production and pollutants degradation under visible light irradiation. Initially, ZnIn$_2$S$_4$/g-C$_3$N$_4$, g-C$_3$N$_4$/CaIn$_2$S$_4$, MoS$_2$/ZnIn$_2$S$_4$ and Fe$_2$O$_3$ or FeOOH doped ZnIn$_2$S$_4$ based heterojunction-type photocatalysts have been studied for the degradation of RhB, MO, 2,4-dichlorophenoxyacetic acid (2,4-D) and 2,4,6-tribromophenol (2,4,6-TBP) [209–212]. However, the separated holes on these composites possess lower oxidation ability. To make use of the high negative CB position of AB$_2$X$_4$, it has been coupled with another semiconductor which has a relatively lower CB position and not able to reduce the O$_2$
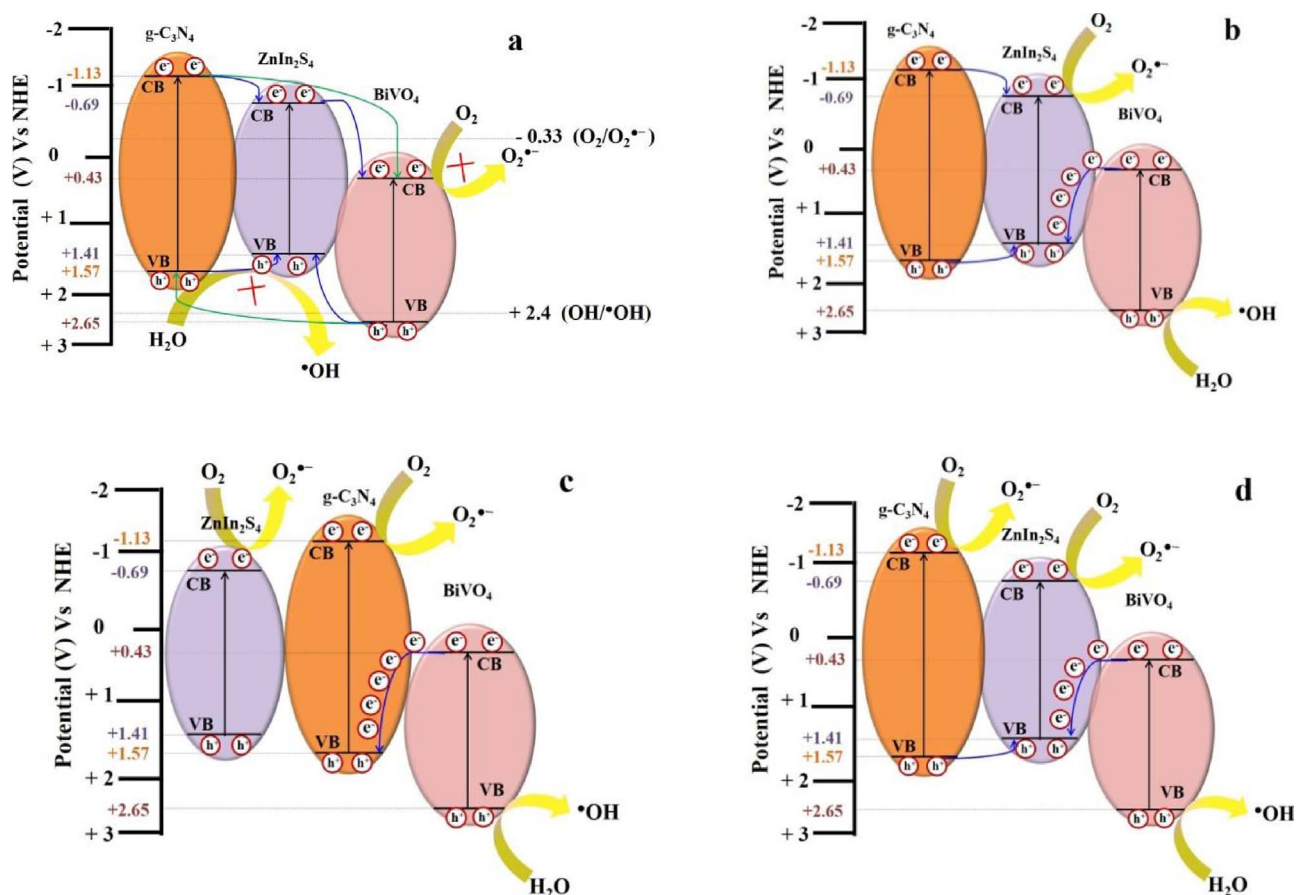

Fig. 12. Schematic representation of electron-hole separation mechanism in ternary nanocomposites (a) heterojunction and (b–d) inter cross sectional electron transfer type. Reprinted with permission from ref. [214].
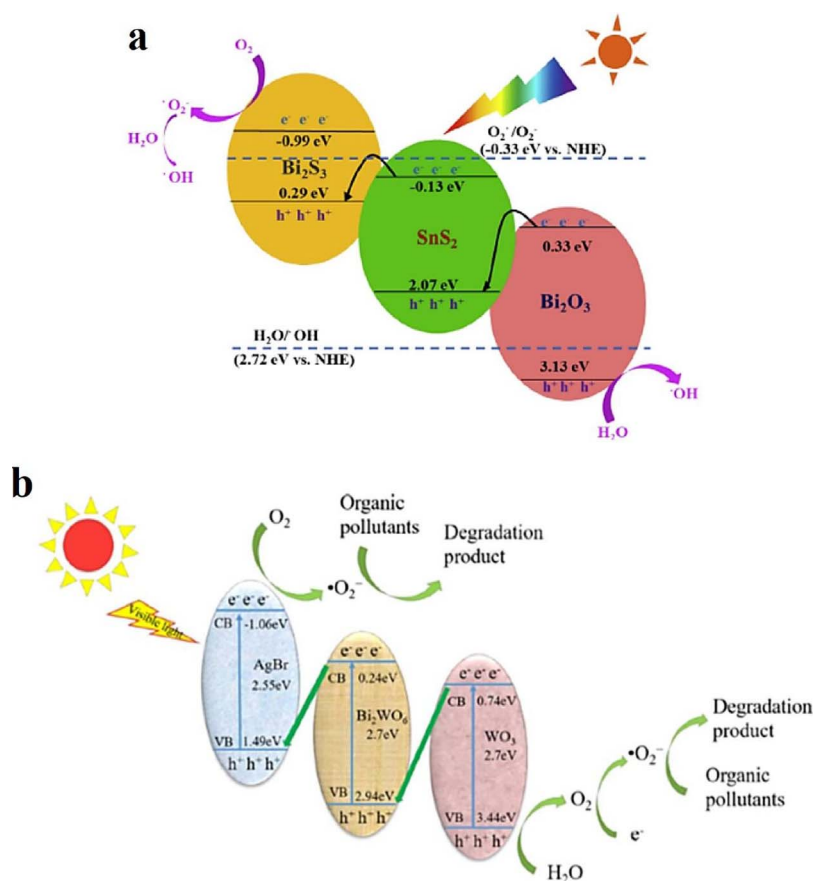
to $O_2^{\cdot-}$ by itself, to obtain a direct dual semiconductor photocatalytic system. Visible light responsive $CaIn_2S_4/TiO_2$ and $ZnIn_2S_4/Bi_2WO_6$ direct dual semiconductors have been prepared by facile wet-impregnation method. The recombination rate on the TiO_2 and Bi_2WO_6 were significantly suppressed by virtue of inter cross sectional electron transport mechanism (Figs. 9b and 10). Thus, the separated electrons on the CB of $CaIn_2S_4$ (-1.1 eV vs NHE) and $ZnIn_2S_4$ (-0.76 eV vs NHE), and the holes on the VB of TiO_2 ($+2.91$ eV vs NHE) and Bi_2WO_6 ($+3.23$ eV vs NHE) were observed to be effectively participating in the degradation of ISN and metronidazole (MTZ) pharmaceutical pollutants [160,167].

Recently double direct dual semiconductor photocatalytic systems have been also developed to further enhance the visible light response and charge carrier separation and transfer rate. Islam et al., proposed that oxygen-vacancy (O_v) rich BiOI act as a self-mediator in $MoS_2/BiOI/AgI$ ternary nanocomposites, wherein charge carriers are separated by transferring the electrons from CB of AgI and MoS_2 to CB of BiOI, and holes on the VB of BiOI transferred to VB of AgI and MoS_2. However, the accumulated holes on the VB of AgI ($+2.43$ eV) and MoS_2 ($+1.81$ eV) and electrons on the CB of BiOI ($+0.50$ eV) cannot generate reactive radicals for further redox reactions. Thus, the electrons on the CB of BiOI travel to oxygen-vacancies and combine with the holes on the VB of MoS_2 and AgI via the inter cross sectional electron transfer mechanism, prolonging the overall lifetime of photo-excited charge carriers (Fig. 11). Thus, the holes on the VB of BiOI ($+2.93$ eV) and electrons on the CB of AgI (-0.47 eV) effectively participates in the catalytic process [213]. We have also prepared $ZnIn_2S_4/g-C_3N_4/BiVO_4$ nanorod-based ternary nanocomposites for congo red (CR) dye and MTZ pharmaceutical degradation. It is revealed that here also charge carriers are efficiently separated through multi inter cross sectional electron transfer mechanism (Fig. 12b–d), which was validated by photoluminescence and reactive radical scavenging studies. The system

displayed ($5\%ZnIn_2S_4$-50%-$g-C_3N_4/BiVO_4$) higher visible light induced photocatalytic degradation activity when compared to the binary composites, $g-C_3N_4$ and $BiVO_4$ [214]. Yu et al., and Zhang et al., synthesized ternary $Bi_2S_3/SnS_2/Bi_2O_3$ and $AgBr/Bi_2WO_6/WO_3$ double dual semiconductor photocatalytic system for dyes (RhB, MO, MB, OG IV, CV) degradation. The lifetime of photogenerated charge carriers on ternary system surface are efficiently improved through inter cross sectional electron transfer mechanism (Fig. 13). Thus, the separated electrons on the CB of Bi_2S_3 and AgBr, holes on the VB Bi_2O_3 and WO_3 are exhibited strong redox ability against dye molecules and exhibited superior photocatalytic activity as compared to binary and unitary photocatalyst [215,216]. Recently various redox-mediator-free direct dual semiconductor photocatalytic materials such as $Ag_4V_2O_7/Ag_3VO_4$, $g-C_3N_4/CoFe_2O_4$, $g-C_3N_4/$perylene imides (PI), $Bi_2MoO_6/BiOBr$, Bi_2MoO_6/Ag_3PO_4, $g-C_3N_4/V_2O_5$, etc., have also been developed for the degradation of RhB, MB, MO, phenol, NO, TC, propylene and CIP pollutants (Table 2). Finally, it is safe to state that to develop novel, efficient and cheap direct dual semiconductor photocatalytic systems, a better understanding of the charge transfer as well as recombination processes taking place at the interface of two specific semiconductors is needed. Understanding the generation and the role of ·OH radicals is also equally important to improve the design of semiconductor combinations and maximise the photocatalytic yield.

6. Conclusion

Photocatalysis has been intensively studied over many decades for the degradation of pollutants. Modifications have been suggested recently to improve the visible light response of photocatalysts and for the enhancement of charge carrier lifetimes. Among those modifications, the development of dual semiconductors with solid-state electron mediators and mediator-free direct dual semiconductor photocatalytic

systems are potentially good for the degradation of pollutants in an efficient manner. Enhanced research effort is still underway to design highly efficient systems of this type. The photogenerated charge carriers are potentially separated over these systems by an inter cross sectional electron transfer mechanism between the two semiconductors, with or without electron-mediators. The literature often compares this type of transfer mechanisms with Z-scheme type water splitting photosynthetic reactions, which mimic natural photosynthesis. However, the usage of Z-scheme concept in photocatalytic pollutant degradation leads to scientific misconceptions and ambiguity as thermodynamically they are distinctly different in term of Gibb's free energy change. Therefore, to respect the scientific definitions or sense when applying a new concept or terminology, it is better to refer them as 'dual semiconductor systems consisting of solid-state electron mediators or without mediators (direct dual semiconductor systems)'. In future, for the development of such systems, the focus should be on finding low band gap single semiconductors with appropriate band edge potentials to produce higher concentration of reactive radical species ($\cdot OH$ and $O_2 \cdot -$). In addition, the charge carrier separation and transfer mechanism occurring on these photocatalysts should be systematically studied. Theoretical calculations and modelling methods are helpful to understand the mechanism in detail. The utilization of direct sunlight by photocatalysts still remains very poor and it is a major challenge ahead for the development of practical sunlight based systems. Moreover, the development of long-term stable and reusable photocatalytic systems should become the top priority to accomplish practical applications required to create a less polluted environment.

Acknowledgments

References

[1] R. Andreozzi, V. Caprio, A. Insola, R. Marotta, Advanced oxidation processes (AOP) for water purification and recovery, Catal. Today 53 (1999) 51–59.

[2] O.K. Dalrymple, D.H. Yeh, M.A. Trotz, Removing pharmaceuticals and endocrine-disrupting compounds from wastewater by photocatalysis, J. Chem. Technol. Biotechnol. 82 (2007) 121–134.

[3] M.M. Khin, A.S. Nair, V.J. Babu, R. Murugan, S. Ramakrishna, A review on nanomaterials for environmental remediation, Energy Environ. Sci. 5 (2012) 8075–8109.

[4] S.C. Markham, Photocatalytic properties of oxides, J. Chem. Educ. 32 (1955) 540.

[5] A. Fujishima, K. Honda, Electrochemical photolysis of water at a semiconductor electrode, Nature 238 (1972) 37–38.

[6] M.R. Hoffmann, S.T. Martin, W. Choi, D.W. Bahnemann, Environmental applications of semiconductor photocatalysis, Chem. Rev. 95 (1995) 69–96.

[7] J. Peral, X. Domènech, D.F. Ollis, Heterogeneous photocatalysis for purification, decontamination and deodorization of air, J. Chem. Technol. Biotechnol. 70 (1997) 117–140.

[8] R.S. Thakur, R. Chaudhary, C. Singh, Fundamentals and applications of the photocatalytic treatment for the removal of industrial organic pollutants and effects of operational parameters:A review, J. Renew. Sustain. Energy 5 (2010) (042701-1-042701-37).

[9] J.A. Byrne, P.A. Fernandez-Ibañez, P.S.M. Dunlop, D.M.A. Alrousan, J.W.J. Hamilton, Photocatalytic enhancement for solar disinfection of water: a review, Int. J. Photoenergy 2011 (2011) 1–12 (Article ID 798051).

[10] L. Rovelli, K.R. Thampi, Solar water splitting using semiconductor systems. Chapter 1, in: Jacinto Sa (Ed.), Fuel Production with Heterogeneous Catalysis, CRC Press, Taylor & Francis Group, 2014, pp. 1–62.

[11] K. Natarajan, T.S. Natarajan, R.I. Kureshy, H.C. Bajaj, W.-K. Jo, R.J. Tayade, Photocatalytic H_2 Production using Semiconductor Nanomaterials via Water Splitting-An Overview, A. Al-Ahmed, M.K. Hossain, M. Afzaal, H.M. Bahaidarah (Eds), Main Theme: Recent Advances in Renewable Energy Research, Periodical: Advan. Mater. Res. Trans Tech Publications Inc., Switzerland, Volume 1116, 2015, pp. 130–156.

[12] P. Usubharatana, D. McMartin, A. Veawab, P. Tontiwachwuthikul, Photocatalytic process for CO_2 emission reduction from industrial flue gas streams, Ind. Eng. Chem. Res. 45 (2006) 2558–2568.

[13] J.H. Carey, J. Lawrence, H.M. Tosine, Photodechlorination of PCB's in the presence of titanium dioxide in aqueous suspensions, Bull. Environ. Contam. Toxicol. 16 (1976) 697–701.

[14] S.N. Frank, A.J. Bard, Heterogeneous photocatalytic oxidation of cyanide ion in aqueous solutions at titanium dioxide powder, J. Am. Chem. Soc. 99 (1977) 303–304.

[15] S.N. Frank, A.J. Bard, Heterogeneous photocatalytic oxidation of cyanide and sulfite in aqueous solutions at semiconductor powders, J. Phys. Chem. 81 (1977) 1484–1488.

[16] R.J. Tayade, R.G. Kulkarni, R.V. Jasra, Photocatalytic degradation of aqueous nitrobenzene by nanocrystalline TiO_2, Ind. Eng. Chem. Res. 45 (2006) 922–927.

[17] C. McCullagh, N. Skillen, M. Adams, P.K.J. Robertson, Photocatalytic reactors for environmental remediation: a review, J. Chem. Technol. Biotechnol. 86 (2011) 1002–1017.

[18] A.A. Ismail, D.W. Bahnemann, Mesoporous titania photocatalysts: preparation, characterization and reaction mechanisms, J. Mater. Chem. 21 (2011) 11686–11707.

[19] T.S. Natarajan, H.C. Bajaj, R.J. Tayade, Preferential adsorption behavior of methylene blue dye onto surface hydroxyl group enriched TiO_2 nanotube and its photocatalytic regeneration, J. Colloid Interfaces Sci. 433 (2014) 104–114.

[20] R.J. Tayade, T.S. Natarajan, H.C. Bajaj, Photocatalytic degradation of methylene blue dye using ultraviolet light emitting diodes, Ind. Eng. Chem. Res. 48 (2009) 10262–10267.

[21] Z. Wang, J. Liu, Y. Dai, W. Dong, S. Zhang, J. Chen, Dimethyl sulfide photocatalytic degradation in a light-emitting-diode continuous reactor: kinetic and mechanistic study, Ind. Eng. Chem. Res. 50 (2011) 7977–7984.

[22] W.-K. Jo, R.J. Tayade, Recent developments in photocatalytic dye degradation upon irradiation with energy-efficient light emitting diodes, Chin. J. Catal. 35 (2014) 1781–1792.

[23] W.-K. Jo, G.T. Park, R.J. Tayade, Synergetic effect of adsorption on degradation of malachite green dye under blue LED irradiation using spiral-shaped photocatalytic reactor, J. Chem. Technol. Biotechnol. 90 (2015) 2280–2289.

[24] M. Pelaez, N.T. Nolan, S.C. Pillai, M.K. Seery, P. Falaras, A.G. Kontos, P.S.M. Dunlop, J.W.J. Hamilton, J.A. Byrne, K. O'Shea, M.H. Entezari, D.D. Dionysiou, A review on the visible light active titanium dioxide photocatalysts for environmental applications, Appl. Catal. B 125 (2012) 331–349.

[25] R.J. Tayade, R.G. Kulkarni, R.V. Jasra, Transition metal ion impregnated mesoporous TiO_2 for photocatalytic degradation of organic contaminants in water, Ind. Eng. Chem. Res. 45 (2006) 5231–5238.

[26] S. Malato, P. Fernández-Ibáñez, M.I. Maldonado, J. Blanco, W. Gernjak, Decontamination and disinfection of water by solar photocatalysis: recent overview and trends, Catal. Today 147 (2009) 1–59.

[27] J. Radjenovic, C. Sirtori, M. Petrović, D. Barceló, S. Malato, Solar photocatalytic degradation of persistent pharmaceuticals at pilot-scale: kinetics and characterization of major intermediate products, Appl. Catal. B 89 (2009) 255–264.

[28] T.S. Natarajan, K. Natarajan, H.C. Bajaj, R.J. Tayade, Enhanced photocatalytic activity of bismuth-doped TiO_2 nanotubes under direct sunlight irradiation for degradation of Rhodamine B dye, J. Nanopart. Res. 15 (1669) (2013) 1–18.

[29] J.A. Sullivan, E.M. Neville, R. Herron, K.R. Thampi, J.M.D. MacElroy, Routes to visible light active C-doped TiO_2 photocatalysts using carbon atoms from the Ti precursors, J. Photochem. Photobiol. A 289 (2014) 60–65.

[30] R. Asahi, T. Morikawa, H. Irie, T. Ohwaki, Nitrogen-Doped titanium dioxide as visible-light-sensitive photocatalyst: designs, developments, and prospects, Chem. Rev. 114 (2014) 9824–9852.

[31] T.S. Natarajan, H.C. Bajaj, R.J. Tayade, Palmyra tuber peel derived activated carbon and anatase TiO_2 nanotube based nanocomposites with enhanced photocatalytic performance in rhodamine 6G dye degradation, Process Safe. Environ. Prot. 104 (2016) 346–357.

[32] K. Natarajan, P. Singh, H.C. Bajaj, R.J. Tayade, Facile synthesis of $TiO_2/ZnFe_2O_4$ nanocomposite by sol-gel auto combustion method for superior visible light photocatalytic efficiency, Korean J. Chem. Eng. 33 (2016) 1788–1798.

[33] T.S. Natarajan, J.Y. Lee, H.C. Bajaj, W.K. Jo, R.J. Tayade, Synthesis of multiwall carbon nanotubes/TiO_2 nanotube composites with enhanced photocatalytic decomposition efficiency, Catal. Today 282 (2017) 13–23.

[34] N. Soltani, E. Saion, M.Z. Hussein, M. Erfani, A. Abedini, G. Bahmanrokh, M. Navasery, P. Vaziri, Visible light-induced degradation of methylene blue in the presence of photocatalytic ZnS and CdS nanoparticles, Int. J. Mol. Sci. 13 (2012) 12242.

[35] S.C. Yan, Z.S. Li, Z.G. Zou, Photodegradation performance of g-C_3N_4 fabricated by directly heating melamine, Langmuir 25 (2009) 10397–10401.

[36] Z. Yi, J. Ye, N. Kikugawa, T. Kako, S. Ouyang, H. Stuart-Williams, H. Yang, J. Cao, W. Luo, Z. Li, Y. Liu, R.L. Withers, An orthophosphate semiconductor with photooxidation properties under visible-light irradiation, Nat. Mater. 9 (2010) 559–564.

[37] T.S. Natarajan, H.C. Bajaj, R.J. Tayade, Synthesis of homogeneous sphere-like Bi_2WO_6 nanostructure by silica protected calcination with high visible-light-driven photocatalytic activity under direct sunlight, CrystEngComm 17 (2015) 1037–1049.

[38] K. Natarajan, H.C. Bajaj, R.J. Tayade, Photocatalytic efficiency of bismuth oxyhalide (Br, Cl and I) nanoplates for RhB dye degradation under LED irradiation, J. Ind. Eng. Chem. 34 (2016) 146–156.

[39] S. Bai, H. Li, Y. Guan, S. Jiang, The enhanced photocatalytic activity of CdS/TiO_2 nanocomposites by controlling CdS dispersion on TiO_2 nanotubes, Appl. Surf. Sci. 257 (2011) 6406–6409.

[40] G. Colon, S. Murcia Lopez, M.C. Hidalgo, J.A. Navio, Sunlight highly photoactive Bi_2WO_6-TiO_2 heterostructures for rhodamine B degradation, Chem. Commun. 46 (2010) 4809–4811.

[41] Y. Hu, D. Li, Y. Zheng, W. Chen, Y. He, Y. Shao, X. Fu, G. Xiao, $BiVO_4/TiO_2$

nanocrystalline heterostructure: a wide spectrum responsive photocatalyst towards the highly efficient decomposition of gaseous benzene, Appl. Catal. B 104 (2011) 30–36.

[42] Z.-h. Yuan, L.-d. Zhang, Synthesis, characterization and photocatalytic activity of ZnFe$_2$O$_4$/TiO$_2$ nanocomposite, J. Mater. Chem. 11 (2001) 1265–1268.

[43] M. Ge, Y. Li, L. Liu, Z. Zhou, W. Chen, Bi$_2$O$_3$-Bi$_2$WO$_6$ composite microspheres: hydrothermal synthesis and photocatalytic performances, J. Phys. Chem. C 115 (2011) 5220–5225.

[44] L. Ge, C. Han, J. Liu, Novel visible light-induced g-C$_3$N$_4$/Bi$_2$WO$_6$ composite photocatalysts for efficient degradation of methyl orange, Appl. Catal. B 108–109 (2011) 100–107.

[45] S. Zhang, J. Li, M. Zeng, G. Zhao, J. Xu, W. Hu, X. Wang, In situ synthesis of water-soluble magnetic graphitic carbon nitride photocatalyst and its synergistic catalytic performance, ACS Appl. Mater. Interfaces 5 (2013) 12735–12743.

[46] L. Ye, J. Liu, Z. Jiang, T. Peng, L. Zan, Facets coupling of BiOBr-g-C$_3$N$_4$ composite photocatalyst for enhanced visible-light-driven photocatalytic activity, Appl. Catal. B 142–143 (2013) 1–7.

[47] Y. Feng, X. Yan, C. Liu, Y. Hong, L. Zhu, M. Zhou, W. Shi, Hydrothermal synthesis of CdS/Bi$_2$MoO$_6$ heterojunction photocatalysts with excellent visible-light-driven photocatalytic performance, Appl. Surf. Sci. 353 (2015) 87–94.

[48] A.J. Bard, Photoelectrochemistry and heterogeneous photo-catalysis at semiconductors, J. Photochem. 10 (1979) 59–75.

[49] K. Sayama, R. Yoshida, H. Kusama, K. Okabe, Y. Abe, H. Arakawa, Photocatalytic decomposition of water into H$_2$ and O$_2$ by a two-step photoexcitation reaction using a WO$_3$ suspension catalyst and an Fe^{3+}/Fe^{2+} redox system, Chem. Phys. Lett. 277 (1997) 387–391.

[50] R. Abe, K. Sayama, K. Domen, H. Arakawa, A new type of water splitting system composed of two different TiO$_2$ photocatalysts (anatase, rutile) and a IO$_3^-$/I$^-$ shuttle redox mediator, Chem. Phys. Lett. 344 (2001) 339–344.

[51] K. Sayama, K. Mukasa, R. Abe, Y. Abe, H. Arakawa, Stoichiometric water splitting into H$_2$ and O$_2$ using a mixture of two different photocatalysts and an IO$_3^-$/I$^-$ shuttle redox mediator under visible light irradiation, Chem. Commun. (2001) 2416–2417.

[52] Y. Sasaki, A. Iwase, H. Kato, A. Kudo, The effect of co-catalyst for Z-scheme photocatalysis systems with an Fe^{3+}/Fe^{2+} electron mediator on overall water splitting under visible light irradiation, J. Catal. 259 (2008) 133–137.

[53] S. Hara, M. Yoshimizu, S. Tanigawa, L. Ni, B. Ohtani, H. Irie, Hydrogen and oxygen evolution photocatalysts synthesized from strontium titanate by controlled doping and their performance in two-step overall water splitting under visible light, J. Phys. Chem. C 116 (2012) 17458–17463.

[54] K. Maeda, Z-Scheme water splitting using two different semiconductor photocatalysts, ACS Catal. 3 (2013) 1486–1503.

[55] H. Li, W. Tu, Y. Zhou, Z. Zou, Z-Scheme photocatalytic systems for promoting photocatalytic performance: recent progress and future challenges, Adv. Sci. 3 (2016) 1500389(1-12).

[56] H. Tada, T. Mitsui, T. Kiyonaga, T. Akita, K. Tanaka, All-solid-state Z-scheme in CdS-Au-TiO$_2$ three-component nanojunction system, Nat. Mater. 5 (2006) 782–786.

[57] C. Hu, Y. Lan, J. Qu, X. Hu, A. Wang, Ag/AgBr/TiO$_2$ visible light photocatalyst for destruction of azodyes and bacteria, J. Phys. Chem. B 110 (2006) 4066–4072.

[58] L. Zhang, K.-H. Wong, Z. Chen, J.C. Yu, J. Zhao, C. Hu, C.-Y. Chan, P.-K. Wong, AgBr-Ag-Bi$_2$WO$_6$ nanojunction system: a novel and efficient photocatalyst with double visible-light active components, Appl. Catal. A 363 (2009) 221–229.

[59] M. Miyauchi, Y. Nukui, D. Atarashi, E. Sakai, Selective growth of n-type nanoparticles on p-type semiconductors for Z-scheme photocatalyst, ACS Appl. Mater. Interfaces 5 (2013) 9770–9776.

[60] T. Arai, M. Yanagida, Y. Konishi, Y. Iwasaki, H. Sugihara, K. Sayama, Efficient complete oxidation of acetaldehyde into CO$_2$ over CuBi$_2$O$_4$/WO$_3$ composite photocatalyst under visible and UV light irradiation, J. Phys. Chem. C 111 (2007) 7574–7577.

[61] C. Shifu, J. Lei, T. Wenming, F. Xianliang, Fabrication, characterization and mechanism of a novel Z-scheme photocatalyst NaNbO$_3$/WO$_3$ with enhanced photocatalytic activity, Dalton Trans. 42 (2013) 10759–10768.

[62] J. Yu, S. Wang, J. Low, W. Xiao, Enhanced photocatalytic performance of direct Z-scheme g-C$_3$N$_4$-TiO$_2$ photocatalysts for the decomposition of formaldehyde in air, Phys. Chem. Chem. Phys. 15 (2013) 16883–16890.

[63] B. Ohtani, Photocatalysis A to Z-What we know and what we do not know in a scientific sense, J. Photochem. Photobiol. C 11 (2010) 157–178.

[64] I.K. Konstantinou, T.A. Albanis, TiO$_2$-assisted photocatalytic degradation of azo dyes in aqueous solution: kinetic and mechanistic investigations: a review, Appl. Catal. B 49 (2004) 1–14.

[65] R.J. Tayade, P.K. Surolia, R.G. Kulkarni, R.V. Jasra, Photocatalytic degradation of dyes and organic contaminants in water using nanocrystalline anatase and rutile TiO$_2$, Sci. Technol. Adv. Mater. 8 (2007) 455–462.

[66] T.S. Natarajan, K. Natarajan, H.C. Bajaj, R.J. Tayade, Study on identification of leather industry wastewater constituents and its photocatalytic treatment, Int. J. Environ. Sci. Technol. 10 (2013) 855–864.

[67] J. Schneider, M. Matsuoka, M. Takeuchi, J. Zhang, Y. Horiuchi, M. Anpo, D.W. Bahnemann, Understanding TiO$_2$ photocatalysis: mechanisms and materials, Chem. Rev. 114 (2014) 9919–9986.

[68] A. Ajmal, I. Majeed, R.N. Malik, H. Idriss, M.A. Nadeem, Principles and mechanisms of photocatalytic dye degradation on TiO$_2$ based photocatalysts: a comparative overview, RSC Adv. 4 (2014) 37003–37026.

[69] P.K. Surolia, R.J. Tayade, R.V. Jasra, Effect of anions on the photocatalytic activity of Fe(III) salts impregnated TiO$_2$, Ind. Eng. Chem. Res. 46 (2007) 6196–6203.

[70] E.M. Neville, M.J. Mattle, D. Loughrey, B. Rajesh, M. Rahman, J.M.D. MacElroy,

J.A. Sullivan, K.R. Thampi, Carbon-doped TiO$_2$ and carbon, tungsten-Co doped TiO$_2$ through Sol–Gel processes in the presence of melamine borate: reflections through photocatalysis, J. Phys. Chem. C 116 (2012) 16511–16521.

[71] R. Daghrir, P. Drogui, D. Robert, Modified TiO$_2$ for environmental photocatalytic applications: a review, Ind. Eng. Chem. Res. 52 (2013) 3581–3599.

[72] E.M. Neville, J.M.D. MacElroy, K.R. Thampi, J.A. Sullivan, Visible light active C-doped titanate nanotubes prepared via alkaline hydrothermal treatment of C-doped nanoparticulate TiO$_2$: Photo-electrochemical and photocatalytic properties, J. Photochem. Photobiol. A 267 (2013) 17–24.

[73] L.G. Devi, R. Kavitha, A review on non metal ion doped titania for the photocatalytic degradation of organic pollutants under UV/solar light: role of photogenerated charge carrier dynamics in enhancing the activity, Appl. Catal. B 140–141 (2013) 559–587.

[74] E.M. Neville, J. Ziegler, J.M. Don MacElroy, K.R. Thampi, J.A. Sullivan, Serendipity following attempts to prepare C-doped rutile TiO$_2$, Appl. Catal. A 470 (2014) 434–441.

[75] S. Leong, A. Razmjou, K. Wang, K. Hapgood, X. Zhang, H. Wang, TiO$_2$ based photocatalytic membranes: a review, J. Membr. Sci. 472 (2014) 167–184.

[76] R. Fagan, D.E. McCormack, D.D. Dionysiou, S.C. Pillai, A review of solar and visible light active TiO$_2$ photocatalysis for treating bacteria, cyanotoxins and contaminants of emerging concern, Mater. Sci. Semicond. Process. 42 (2016) 2–14.

[77] I. Medina-Ramírez, J.L. Liu, A. Hernández-Ramírez, C. Romo-Bernal, G. Pedroza-Herrera, J. Jáuregui-Rincón, M.A. Gracia-Pinilla, Synthesis, characterization, photocatalytic evaluation, and toxicity studies of TiO$_2$–Fe^{3+} nanocatalyst, J. Mater. Sci. 49 (2014) 5309–5323.

[78] E.P. Reddy, L. Davydov, P. Smirniotis, TiO$_2$-loaded zeolites and mesoporous materials in the sonophotocatalytic decomposition of aqueous organic pollutants: the role of the support, Appl. Catal. B 42 (2003) 1–11.

[79] R.J. Tayade, R.G. Kulkarni, R.V. Jasra, Enhanced photocatalytic activity of TiO$_2$-coated NaY and HY zeolites for the degradation of methylene blue in water, Ind. Eng. Chem. Res. 46 (2007) 369–376.

[80] G.L. Puma, A. Bono, D. Krishnaiah, J.G. Collin, Preparation of titanium dioxide photocatalyst loaded onto activated carbon support using chemical vapor deposition: a review paper, J. Hazard. Mater. 157 (2008) 209–219.

[81] R.J. Tayade, P.K. Surolia, M.A. Lazar, R.V. Jasra, Enhanced photocatalytic activity by silver metal ion exchanged NaY zeolite photocatalysts for the degradation of organic contaminants and dyes in aqueous medium, Ind. Eng. Chem. Res. 47 (2008) 7545–7551.

[82] R. Leary, A. Westwood, Carbonaceous nanomaterials for the enhancement of TiO$_2$ photocatalysis, Carbon 49 (2011) 741–772.

[83] K.M. Garadkar, A.A. Patil, P.P. Hankare, P.A. Chate, D.J. Sathe, S.D. Delekar, MoS$_2$. Preparation and their characterization, J. Alloys Compd. 487 (2009) 786–789.

[84] L. Zhang, W. Wang, Z. Chen, L. Zhou, H. Xu, W. Zhu, Fabrication of flower-like Bi$_2$WO$_6$ superstructures as high performance visible-light driven photocatalysts, J. Mater. Chem. 17 (2007) 2526–2532.

[85] H. An, Y. Du, T. Wang, C. Wang, W. Hao, J. Zhang, Photocatalytic properties of BiOX (X = Cl, Br, and I), Rare Met. 27 (2008) 243–250.

[86] G. Mamba, A. Mishra, Advances in magnetically separable photocatalysts: smart, recyclable materials for water pollution mitigation, Catalysts 6 (79) (2016) 1–34.

[87] K. Ranjit, B. Viswanathan, Synthesis, characterization and photocatalytic properties of iron-doped TiO$_2$ catalysts, J. Photochem. Photobiol. A 108 (1997) 79–84.

[88] J. Low, J. Yu, M. Jaroniec, S. Wageh, A.A. Al-Ghamdi, Heterojunction photocatalysts, Adv. Mater. 29 (2017) 1–20 (1601694).

[89] X. Ma, Q. Jiang, W. Guo, M. Zheng, W. Xu, F. Ma, B. Hou, Fabrication of g-C$_3$N$_4$/Au/CdZnS Z-scheme photocatalyst to enhance photocatalysis performance, RSC Adv. 6 (2016) 28263–28269.

[90] D. Lu, H. Wang, X. Zhao, K.K. Kondamareddy, J. Ding, C. Li, P. Fang, Highly efficient visible-light-induced photoactivity of Z-scheme g-C$_3$N$_4$/Ag/MoS$_2$ ternary photocatalysts for organic pollutant degradation and production of hydrogen, ACS Sustain. Chem. Eng. 5 (2017) 1436–1445.

[91] W.-K. Jo, N.C.S. Selvam, Z-scheme CdS/g-C$_3$N$_4$ composites with RGO as an electron mediator for efficient photocatalytic H$_2$ production and pollutant degradation, Chem. Eng. J. 317 (2017) 913–924.

[92] G. Zhao, X. Huang, F. Fina, G. Zhang, J.T.S. Irvine, Facile structure design based on C$_3$N$_4$ for mediator-free Z-scheme water splitting under visible light, Catal. Sci. Technol. 5 (2015) 3416–3422.

[93] F.Q. Zhou, J.C. Fan, Q.J. Xu, Y.L. Min, BiVO$_4$ nanowires decorated with CdS nanoparticles as Z-scheme photocatalyst with enhanced H2 generation, Appl. Catal. B 201 (2017) 77–83.

[94] H. Zhu, B. Yang, J. Xu, Z. Fu, M. Wen, T. Guo, S. Fu, J. Zuo, S. Zhang, Construction of Z-scheme type CdS–Au–TiO$_2$ hollow nanorod arrays with enhanced photocatalytic activity, Appl. Catal. B 90 (2009) 463–469.

[95] H. Lin, J. Cao, B. Luo, B. Xu, S. Chen, Synthesis of novel Z-scheme AgI/Ag/AgBr composite with enhanced visible light photocatalytic activity, Catal. Comm. 21 (2012) 91–95.

[96] Z. Chen, W. Wang, Z. Zhang, X. Fang, High-efficiency visible-light-driven Ag$_3$PO$_4$/AgI photocatalysts: z-scheme photocatalytic mechanism for their enhanced photocatalytic activity, J. Phys. Chem. C 117 (2013) 19346–19352.

[97] J. Song, J. Shi, M. Ren, G. Hu, Synthesis, characterization and excellent photocatalytic activity of Ag/AgBr/MoO$_3$ composite photocatalyst, Appl. Phys. A 116 (2014) 2139–2147.

[98] H. Katsumata, T. Hayashi, M. Taniguchi, T. Suzuki, S. Kaneco, Highly efficient visible-light driven AgBr/Ag$_3$PO$_4$ hybrid photocatalysts with enhanced photocatalytic activity, Mater. Sci. Semicond. Process 25 (2014) 68–75.

[99] Y. Min, G. He, Q. Xu, Y. Chen, Self-assembled encapsulation of graphene oxide/Ag@AgCl as a Z-scheme photocatalytic system for pollutant removal, J. Mater. Chem. A 2 (2014) 1294–1301.

[100] Y. Yang, W. Guo, Y. Guo, Y. Zhao, X. Yuan, Y. Guo, Fabrication of Z-scheme plasmonic photocatalyst Ag@AgBr/g-C$_3$N$_4$ with enhanced visible-light photocatalytic activity, J. Hazard. Mater. 271 (2014) 150–159.

[101] L. Shi, L. Liang, F. Wang, M. Liu, J. Sun, Enhanced visible-light photocatalytic activity and stability over g-C$_3$N$_4$/Ag$_2$CO$_3$ composites, J. Mater. Sci. 50 (2015) 1718–1727.

[102] W. Li, C. Feng, S. Dai, J. Yue, F. Hua, H. Hou, Fabrication of sulfur-doped g-C$_3$N$_4$/Au/CdS Z-scheme photocatalyst to improve the photocatalytic performance under visible light, Appl. Catal. B 168–169 (2015) 465–471.

[103] R. Xie, L. Zhang, H. Xu, Y. Zhong, X. Sui, Z. Mao, Fabrication of Z-scheme photocatalyst Ag–AgBr@Bi$_{20}$TiO$_{32}$ and its visible-light photocatalytic activity for the degradation of isoproturon herbicide, J. Mol. Catal. A: Chem. 406 (2015) 194–203.

[104] Z. Chen, F. Bing, Q. Liu, Z. Zhang, X. Fang, Novel Z-scheme visible-light-driven Ag$_3$PO$_4$/Ag/SiC photocatalysts with enhanced photocatalytic activity, J. Mater. Chem. A 3 (2015) 4652–4658.

[105] Y. Bu, Z. Chen, C. Sun, Highly efficient Z-Scheme Ag$_3$PO$_4$/Ag/WO$_{3-x}$ photocatalyst for its enhanced photocatalytic performance, Appl. Catal. B 179 (2015) 363–371.

[106] J. Li, Y. Xie, Y. Zhong, Y. Hu, Facile synthesis of Z-scheme Ag$_2$CO$_3$/Ag/AgBr ternary heterostructured nanorods with improved photostability and photoactivity, J. Mater. Chem. A 3 (2015) 5474–5481.

[107] J. Li, H. Yuan, Z. Zhu, Fabrication of Cu$_2$O/Au/BiPO$_4$ Z-scheme photocatalyst to improve the photocatalytic activity under solar light, J. Mol. Catal. A: Chem. 410 (2015) 133–139.

[108] Y. Wang, C.-G. Niu, L. Zhang, Y. Wang, H. Zhang, D.-W. Huang, X.-G. Zhang, L. Wang, G.-M. Zeng, High-efficiency visible-light AgI/Ag/Bi$_2$MoO$_6$ as a Z-scheme photocatalyst for environmental applications, RSC Adv. 6 (2016) 10221–10228.

[109] Q. Yang, F. Chen, X. Li, D. Wang, Y. Zhong, G. Zeng, Self-assembly Z-scheme heterostructured photocatalyst of Ag$_2$O@Ag-modified bismuth vanadate for efficient photocatalytic degradation of single and dual organic pollutants under visible light irradiation, RSC Adv. 6 (2016) 60291–60307.

[110] D. Ma, J. Wu, M. Gao, Y. Xin, T. Ma, Y. Sun, Fabrication of Z-scheme g-C$_3$N$_4$/RGO/Bi$_2$WO$_6$ photocatalyst with enhanced visible-light photocatalytic activity, Chem. Eng. J. 290 (2016) 136–146.

[111] Q. Shi, W. Zhao, L. Xie, J. Chen, M. Zhang, Y. Li, Enhanced visible-light driven photocatalytic mineralization of indoor toluene via a BiVO$_4$/reduced graphene oxide/Bi$_2$O$_3$ all-solid-state Z-scheme system, J. Alloys Compd. 662 (2016) 108–117.

[112] Y. Bai, T. Chen, P. Wang, L. Wang, L. Ye, X. Shi, W. Bai, Size-dependent role of gold in g-C$_3$N$_4$/BiOBr/Au system for photocatalytic CO$_2$ reduction and dye degradation, Sol. Energy Mater. Sol. Cells 157 (2016) 406–414.

[113] J. Li, H. Yuan, Z. Zhu, Photoelectrochemical performance of g-C$_3$N$_4$/Au/BiPO$_4$ Z-scheme composites to improve the mineralization property under solar light, RSC Adv. 6 (2016) 70563–70572.

[114] C. Zhu, L. Zhang, B. Jiang, J. Zheng, P. Hu, S. Li, M. Wu, W. Wu, Fabrication of Z-scheme Ag$_3$PO$_4$/MoS$_2$ composites with enhanced photocatalytic activity and stability for organic pollutant degradation, Appl. Surf. Sci. 377 (2016) 99–108.

[115] D. Peng, H. Wang, K. Yu, Y. Chang, X. Ma, S. Dong, Photochemical preparation of the ternary composite CdS/Au/g-C$_3$N$_4$ with enhanced visible light photocatalytic performance and its microstructure, RSC Adv. 6 (2016) 77760–77767.

[116] M. Yan, F. Zhu, W. Gu, L. Sun, W. Shi, Y. Hua, Construction of nitrogen-doped graphene quantum dots-BiVO$_4$/g-C$_3$N$_4$ Z-scheme photocatalyst and enhanced photocatalytic degradation of antibiotics under visible light, RSC Adv. 6 (2016) 61162–61174.

[117] H. Li, H. Yu, X. Quan, S. Chen, Y. Zhang, Uncovering the key role of the fermi level of the electron mediator in a Z-scheme photocatalyst by detecting the charge transfer process of WO$_3$-metal-gC$_3$N$_4$ (Metal = Cu, Ag Au), ACS Appl. Mater. Interfaces 8 (2016) 2111–2119.

[118] F. Chen, Q. Yang, X. Li, G. Zeng, D. Wang, C. Niu, J. Zhao, H. An, T. Xie, Y. Deng, Hierarchical assembly of graphene-bridged Ag$_3$PO$_4$/Ag/BiVO$_4$ (040) Z-scheme photocatalyst: an efficient, sustainable and heterogeneous catalyst with enhanced visible-light photoactivity towards tetracycline degradation under visible light irradiation, Appl. Catal. B 200 (2017) 330–342.

[119] D. Ma, J. Wu, M. Gao, Y. Xin, Y. Sun, T. Ma, Hydrothermal synthesis of an artificial Z-scheme visible light photocatalytic system using reduced graphene oxide as the electron mediator, Chem. Eng. J. 313 (2017) 1567–1576.

[120] L. Zhou, W. Zhang, L. Chen, H. Deng, Z-scheme mechanism of photogenerated carriers for hybrid photocatalyst Ag$_3$PO$_4$/g-C$_3$N$_4$ in degradation of sulfamethoxazole, J. Colloid Interfaces Sci. 487 (2017) 410–417.

[121] J. He, D.W. Shao, L.C. Zheng, L.J. Zheng, D.Q. Feng, J.P. Xu, X.H. Zhang, W.C. Wang, W.H. Wang, F. Lu, H. Dong, Y.H. Cheng, H. Liu, R.K. Zheng, Construction of Z-scheme Cu$_2$O/Cu/AgBr/Ag photocatalyst with enhanced photocatalytic activity and stability under visible light, Appl. Catal. B 203 (2017) 917–926.

[122] W. Shi, F. Guo, S. Yuan, In situ synthesis of Z-scheme Ag$_3$PO$_4$/CuBi$_2$O$_4$ photocatalysts and enhanced photocatalytic performance for the degradation of tetracycline under visible light irradiation, Appl. Catal. B 209 (2017) 720–728.

[123] F. Wu, X. Li, W. Liu, S. Zhang, Highly enhanced photocatalytic degradation of methylene blue over the indirect all-solid-state Z-scheme g-C$_3$N$_4$-RGO-TiO$_2$ nanoheterojunctions, Appl. Surf. Sci. 405 (2017) 60–70.

[124] J. Luo, X. Zhou, X. Ning, L. Zhan, L. Ma, X. Xu, Z. Huang, J. Liang, Synthesis and characterization of Z-scheme In$_2$S$_3$/Ag$_2$CrO$_4$ composites with an enhanced visible-light photocatalytic performance, New J. Chem. 41 (2017) 845–856.

[125] S. Bao, Q. Wu, S. Chang, B. Tian, J. Zhang, Z-scheme CdS-Au-BiVO$_4$ with enhanced photocatalytic activity for organic contaminant decomposition, Catal. Sci. Technol. 7 (2017) 124–132.

[126] D. Wang, H. Shen, L. Guo, F. Fu, Y. Liang, Design and construction of the sandwich-like Z-scheme multicomponent CdS/Ag/Bi$_2$MoO$_6$ heterostructure with enhanced photocatalytic performance in RhB photodegradation, New J. Chem. 40 (2016) 8614–8624.

[127] N. Wei, H. Cui, M. Wang, X. Wang, X. Song, L. Ding, J. Tian, Highly efficient photocatalytic activity of Ag$_3$PO$_4$/Au/ZnS(en)$_{0.5}$ photocatalysts through Z-scheme photocatalytic mechanism, RSC Adv. 7 (2017) 18392–18399.

[128] D. Ma, J. Wu, M. Gao, Y. Xin, C. Chai, Enhanced debromination and degradation of 2,4-dibromophenol by an Z-scheme Bi$_2$MoO$_6$/CNTs/g-C$_3$N$_4$ visible light photocatalyst, Chem. Eng. J. 316 (2017) 461–470.

[129] C. Zhang, K. Yu, Y. Feng, Y. Chang, T. Yang, Y. Xuan, D. Lei, L.-L. Lou, S. Liu, Novel 3DOM-SrTiO$_3$/Ag/Ag$_3$PO$_4$ ternary Z-scheme photocatalysts with remarkably improved activity and durability for contaminant degradation, Appl. Catal. B 210 (2017) 77–87.

[130] X. Zheng, Z. Wang, G. Wang, T.R. Gengenbach, D.T. McCarthy, A. Deletic, J. Yu, X. Zhang, Highly dispersed TiO$_2$ nanocrystals and WO$_3$ nanorods on reduced graphene oxide: z-scheme photocatalysis system for accelerated photocatalytic water disinfection, Appl. Catal. B 218 (2017) 163–173.

[131] Q. Li, Z. Quan, D. Wu, X. Zhao, S. Bao, B. Tian, J. Zhang, Z-scheme BiOCl-Au-CdS heterostructure with enhanced sunlight- driven photocatalytic activity in degrading water dyes and antibiotics, ACS Sustain. Chem. Eng. 5 (2017) 6958–6968.

[132] Y. Gong, X. Quan, H. Yu, S. Chen, Synthesis of Z-scheme Ag$_2$CrO$_4$/Ag/g-C$_3$N$_4$ composite with enhanced visible-light photocatalytic activity for 2,4-dichlorophenol degradation, Appl. Catal. B 219 (2017) 439–449.

[133] Z. Song, Y. He, Novel AgCl/Ag/AgFeO$_2$ Z-scheme heterostructure photocatalyst with enhanced photocatalytic and stability under visible light, Appl. Surf. Sci. 420 (2017) 911–918.

[134] J. Zhang, Y. Guo, Y. Xiong, D. Zhou, S. Dong, An environmentally friendly Z-scheme WO$_3$/CDots/CdS heterostructure with remarkable photocatalytic activity and anti-photocorrosion performance, J. Catal. 356 (2017) 1–13.

[135] Y. Xu, Q. Liu, C. Liu, Y. Zhai, M. Xie, L. Huang, H. Xu, H. Li, J. Jiang, Visible-light-driven Ag/AgBr/ZnFe$_2$O$_4$ composites with excellent photocatalytic activity for E. coli disinfection and organic pollutant degradation, J. Colloid Interfaces Sci. 512 (2018) 555–566.

[136] X. Yuan, L. Jiang, X. Chen, L. Leng, H. Wang, Z. Wu, T. Xiong, J. Liang, G. Zeng, Highly efficient visible-light-induced photoactivity of Z-scheme Ag$_2$CO$_3$/Ag/WO$_3$ photocatalysts for organic pollutant degradation, Environ. Sci.: Nano 4 (2017) 2175–2185.

[137] A. Iwase, Y.H. Ng, Y. Ishiguro, A. Kudo, R. Amal, Reduced graphene oxide as a solid-state electron mediator in Z-scheme photocatalytic water splitting under visible light, J. Am. Chem. Soc. 133 (2011) 11054–11057.

[138] T. Arai, M. Yanagida, Y. Konishi, Y. Iwasaki, H. Sugihara, K. Sayama, Promotion effect of CuO co-catalyst on WO$_3$-catalyzed photodegradation of organic substances, Catal. Commun. 9 (2008) 1254–1258.

[139] T. Arai, M. Horiguchi, M. Yanagida, T. Gunji, H. Sugihara, K. Sayama, Reaction mechanism and activity of WO$_3$-catalyzed photodegradation of organic substances promoted by a CuO cocatalyst, J. Phys. Chem. C 113 (2009) 6602–6609.

[140] S. Chen, Y. Hu, L. Ji, X. Jiang, X. Fu, Preparation and characterization of direct Z-scheme photocatalyst Bi$_2$O$_3$/NaNbO$_3$ and its reaction mechanism, Appl. Surf. Sci. 292 (2014) 357–366.

[141] W.-J. Ong, L.-L. Tan, Y.H. Ng, S.-T. Yong, S.-P. Chai, Graphitic carbon nitride (g-C$_3$N$_4$)-based photocatalysts for artificial photosynthesis and environmental remediation: are we a step closer to achieving sustainability? Chem. Rev. 116 (2016) 7159–7329.

[142] J. Wen, J. Xie, X. Chen, X. Li, A review on g-C$_3$N$_4$-based photocatalysts, Appl. Surf. Sci. 391 (2017) 72–123.

[143] S. Chen, Y. Hu, S. Meng, X. Fu, Study on the separation mechanisms of photogenerated electrons and holes for composite photocatalysts g-C$_3$N$_4$-WO$_3$, Appl. Catal. B 150–151 (2014) 564–573.

[144] S. Kumar, A. Baruah, S. Tonda, B. Kumar, V. Shanker, B. Sreedhar, Cost-effective and eco-friendly synthesis of novel and stable N-doped ZnO/g-C$_3$N$_4$ core-shell nanoplates with excellent visible-light responsive photocatalysis, Nanoscale 6 (2014) 4830–4842.

[145] X. Chen, X. Huang, Z. Yi, Enhanced ethylene photodegradation performance of g-C$_3$N$_4$–Ag$_3$PO$_4$ composites with direct Z-scheme configuration, Chem. Eur. J. 20 (2014) 17590–17596.

[146] J. Zhang, Y. Hu, X. Jiang, S. Chen, S. Meng, X. Fu, Design of a direct Z-scheme photocatalyst: preparation and characterization of Bi$_2$O$_3$/g-C$_3$N$_4$ with high visible light activity, J. Hazard. Mater. 280 (2014) 713–722.

[147] Y. Bai, P.-Q. Wang, J.-Y. Liu, X.-J. Liu, Enhanced photocatalytic performance of direct Z-scheme BiOCl-g-C$_3$N$_4$ photocatalysts, RSC Adv. 4 (2014) 19456–19461.

[148] Y. He, L. Zhang, B. Teng, M. Fan, Enhanced photodegradation activity of methyl orange over Z-scheme type MoO$_3$-g-C$_3$N$_4$ composite under visible light irradiation, RSC Adv. 4 (2014) 13610–13619.

[149] Y. Su, J. Lang, N. Cao, T. Wang, B. Zhu, X. Wang, Morphological reconstruction and photocatalytic enhancement of NaTaO$_3$ nanocrystals via Cu$_2$O loading, J. Nanopart. Res. 17 (63) (2015) 1–9.

[150] D. Xu, B. Cheng, S. Cao, J. Yu, Enhanced photocatalytic activity and stability of Z-scheme Ag$_2$CrO$_4$-GO composite photocatalysts for organic pollutant degradation, Appl. Catal. B 164 (2015) 380–388.

[151] Z. Zhang, D. Jiang, C. Xing, L. Chen, M. Chen, M. He, Novel AgI-decorated β-Bi$_2$O$_3$ nanosheet heterostructured Z-scheme photocatalysts for efficient degradation of organic pollutants with enhanced performance, Dalton Trans. 44 (2015)

11582–11591.

[152] W. Liao, M. Murugananthan, Y. Zhang, Synthesis of Z-scheme g-C$_3$N$_4$-Ti^{3+}/TiO$_2$ material: an efficient visible light photoelectrocatalyst for degradation of phenol, Phys. Chem. Chem. Phys. 17 (2015) 8877–8884.

[153] W. Zhang, X. Xiao, L. Zheng, C. Wan, Fabrication of TiO$_2$/MoS$_2$@zeolite photocatalyst and its photocatalytic activity for degradation of methyl orange under visible light, Appl. Surf. Sci. 358 (2015) 468–478.

[154] Y. Zheng, G. Chen, Y. Yu, J. Sun, Y. Zhou, F. He, Ion exchange synthesis of an all tungsten based Z-scheme photocatalytic system with highly enhanced photocatalytic activity, RSC Adv. 5 (2015) 46897–46903.

[155] W.K. Jo, T.S. Natarajan, Influence of TiO$_2$ morphology on the photocatalytic efficiency of direct Z-scheme g-C$_3$N$_4$/TiO$_2$ photocatalysts for isoniazid degradation, Chem. Eng. J 281 (2015) 549–565.

[156] N. Tian, H. Huang, Y. He, Y. Guo, T. Zhang, Y. Zhang, Mediator-free direct Z-scheme photocatalytic system: BiVO$_4$/g-C$_3$N$_4$ organic-inorganic hybrid photocatalyst with highly efficient visible-light-induced photocatalytic activity, Dalton Trans. 44 (2015) 4297–4307.

[157] J. Lv, K. Dai, J. Zhang, L. Geng, C. Liang, Q. Liu, G. Zhu, C. Chen, Facile synthesis of Z-scheme graphitic-C$_3$N$_4$/Bi$_2$MoO$_6$ nanocomposite for enhanced visible photocatalytic properties, Appl. Surf. Sci. 358 (2015) 377–384.

[158] W. Chen, T.-Y. Liu, T. Huang, X.-H. Liu, J.-W. Zhu, G.-R. Duan, X.-J. Yang, In situ fabrication of novel Z-scheme Bi$_2$WO$_6$ quantum dots/g-C$_3$N$_4$ ultrathin nanosheets heterostructures with improved photocatalytic activity, Appl. Surf. Sci. 355 (2015) 379–387.

[159] I. Aslam, C. Cao, M. Tanveer, M.H. Farooq, W.S. Khan, M. Tahir, F. Idrees, S. Khalid, A novel Z-scheme WO$_3$/CdWO$_4$ photocatalyst with enhanced visible-light photocatalytic activity for the degradation of organic pollutants, RSC Adv. 5 (2015) 6019–6026.

[160] W.K. Jo, T.S. Natarajan, Facile synthesis of novel redox-mediator-free direct Z-scheme CaIn$_2$S$_4$ marigold-flower-like/TiO$_2$ photocatalysts with superior photocatalytic efficiency, ACS Appl. Mater. Interfaces 7 (2015) 17138–17154.

[161] Y. Liu, R. Wang, Z. Yang, H. Du, Y. Jiang, C. Shen, K. Liang, A. Xu, Enhanced visible-light photocatalytic activity of Z-scheme graphitic carbon nitride/oxygen vacancy-rich zinc oxide hybrid photocatalysts, Chin. J. Catal. 36 (2015) 2135–2144.

[162] S. Meng, X. Ning, T. Zhang, S.-F. Chen, X. Fu, What is the transfer mechanism of photogenerated carriers for the nanocomposite photocatalyst Ag$_3$PO$_4$/g-C$_3$N$_4$, band–band transfer or a direct Z-scheme? Phys. Chem. Chem. Phys. 17 (2015) 11577–11585.

[163] S. Chen, Y. Hu, X. Jiang, S. Meng, X. Fu, Fabrication and characterization of novel Z-scheme photocatalyst WO$_3$/g-C$_3$N$_4$ with high efficient visible light photocatalytic activity, Mater. Chem. Phys. 149–150 (2015) 512–521.

[164] A. Samal, D.P. Das, K.K. Nanda, B.K. Mishra, J. Das, A. Dash, Reduced graphene oxide-Ag$_3$PO$_4$ heterostructure: a direct Z-Scheme photocatalyst for augmented photoreactivity and stability, Chem. Asian J. 11 (2016) 584–595.

[165] M.J. Islam, D.A. Reddy, J. Choi, T.K. Kim, Surface oxygen vacancy assisted electron transfer and shuttling for enhanced photocatalytic activity of a Z-scheme CeO$_2$-AgI nanocomposite, RSC Adv. 6 (2016) 19341–19350.

[166] Y. Hong, Y. Jiang, C. Li, W. Fan, X. Yan, M. Yan, W. Shi, In-situ synthesis of direct solid-state Z-scheme V$_2$O$_5$/g-C$_3$N$_4$ heterojunctions with enhanced visible light efficiency in photocatalytic degradation of pollutants, Appl. Catal. B 180 (2016) 663–673.

[167] W.K. Jo, J.Y. Lee, T.S. Natarajan, Fabrication of hierarchically structured novel redox-mediator-free ZnIn$_2$S$_4$ marigold flower/Bi$_2$WO$_6$ flower-like direct Z-scheme nanocomposite photocatalysts with superior visible light photocatalytic efficiency, Phys. Chem. Chem. Phys. 18 (2016) 1000–1016.

[168] Z. Wang, J. lv, K. Dai, C. Lu, C. Liang, L. Geng, Large scale and facile synthesis of novel Z-scheme Bi$_2$MoO$_6$/Ag$_3$PO$_4$ composite for enhanced visible light photocatalyst, Mater. Lett. 169 (2016) 250–253.

[169] B. Chen, P. Li, S. Zhang, W. Zhang, X. Dong, F. Xi, J. Liu, The enhanced photocatalytic performance of Z-scheme two-dimensional/two-dimensional heterojunctions from graphitic carbon nitride nanosheets and titania nanosheets, J. Colloid Interfaces Sci. 478 (2016) 263–270.

[170] T. Wang, W. Quan, D. Jiang, L. Chen, D. Li, S. Meng, M. Chen, Synthesis of redox-mediator-free direct Z-scheme AgI/WO$_3$ nanocomposite photocatalysts for the degradation of tetracycline with enhanced photocatalytic activity, Chem. Eng. J. 300 (2016) 280–290.

[171] C. Ren, J. Fan, S. Liu, W. Li, F. Wang, H. Li, X. Liu, Z. Chang, One-step hydrothermal synthesis of novel Ag$_3$VO$_4$/Ag$_4$V$_2$O$_7$ composites for enhancing visible-light photocatalytic performance, RSC Adv. 6 (2016) 95156–95164.

[172] K. Li, X. Zeng, S. Gao, L. Ma, Q. Wang, H. Xu, Z. Wang, B. Huang, Y. Dai, J. Lu, Ultrasonic-assisted pyrolyzation fabrication of reduced SnO$_{2-x}$/g-C$_3$N$_4$ heterojunctions: enhance photoelectrochemical and photocatalytic activity under visible LED light irradiation, Nano Res. 9 (2016) 1969–1982.

[173] Y. Deng, L. Tang, G. Zeng, J. Wang, Y. Zhou, J. Wang, J. Tang, Y. Liu, B. Peng, F. Chen, Facile fabrication of a direct Z-scheme Ag$_2$CrO$_4$/g-C$_3$N$_4$ photocatalyst with enhanced visible light photocatalytic activity, J. Mol. Catal. A: Chem. 421 (2016) 209–221.

[174] Y. Yao, G. Wu, F. Lu, S. Wang, Y. Hu, J. Zhang, W. Huang, F. Wei, Enhanced photo-Fenton-like process over Z-scheme CoFe$_2$O$_4$/g-C$_3$N$_4$ Heterostructures under natural indoor light, Environ. Sci. Pollut. Res. 23 (2016) 21833–21845.

[175] G. Dong, L. Yang, F. Wang, L. Zang, C. Wang, Removal of nitric oxide through visible light photocatalysis by g-C$_3$N$_4$ modified with perylene imides, ACS Catal. 6 (2016) 6511–6519.

[176] S. Li, X. Gu, Y. Zhao, Y. Qiang, S. Zhang, M. Sui, Enhanced visible-light photocatalytic activity and stability by incorporating a small amount of MoS$_2$ into

[177] Ag$_3$PO$_4$ microcrystals, J. Mater. Sci.: Mater. Electron. 27 (2016) 386–392.

C. Song, Y. Feng, W. Shi, C. Liu, Fabrication and mechanism of a novel direct solid-state Z-scheme photocatalyst CdS/BiOI under visible light, CrystEngComm 18 (2016) 7796–7804.

[178] D. Zhou, Z. Chen, Q. Yang, X. Dong, J. Zhang, L. Qin, In-situ construction of all-solid-state Z-scheme g-C$_3$N$_4$/TiO$_2$ nanotube arrays photocatalyst with enhanced visible-light-induced properties, Sol. Energy Mater. Sol. Cells 157 (2016) 399–405.

[179] J. Lu, Y. Wang, F. Liu, L. Zhang, S. Chai, Fabrication of a direct Z-scheme type WO$_3$/Ag$_3$PO$_4$ composite photocatalyst with enhanced visible-light photocatalytic performances, Appl. Surf. Sci. 393 (2017) 180–190.

[180] Y. Li, K. Lv, W. Ho, F. Dong, X. Wu, Y. Xia, Hybridization of rutile TiO$_2$ (rTiO$_2$) with g-C$_3$N$_4$ quantum dots (CN QDs): An efficient visible-light-driven Z-scheme hybridized photocatalyst, Appl. Catal. B 202 (2017) 611–619.

[181] B. Zhu, P. Xia, Y. Li, W. Ho, J. Yu, Fabrication and photocatalytic activity enhanced mechanism of direct Z-scheme g-C$_3$N$_4$/Ag$_2$WO$_4$ photocatalyst, Appl. Surf. Sci. 391 (2017) 175–183.

[182] J. Li, M. Zhang, Q. Li, J. Yang, Enhanced visible light activity on direct contact Z-scheme g-C$_3$N$_4$-TiO$_2$ photocatalyst, Appl. Surf. Sci. 391 (2017) 184–193.

[183] F. Wang, W. Li, S. Gu, H. Li, X. Wu, C. Ren, X. Liu, Facile fabrication of direct Z-scheme MoS$_2$/Bi$_2$WO$_6$ heterojunction photocatalyst with superior photocatalytic performance under visible light irradiation, J. Photochem. Photobiol. A 335 (2017) 140–148.

[184] S. Wang, X. Yang, X. Zhang, X. Ding, Z. Yang, K. Dai, H. Chen, A plate-on-plate sandwiched Z-scheme heterojunction photocatalyst: BiOBr-Bi$_2$MoO$_6$ with enhanced photocatalytic performance, Appl. Surf. Sci. 391 (2017) 194–201.

[185] L. Cui, X. Ding, Y. Wang, H. Shi, L. Huang, Y. Zuo, S. Kang, Facile preparation of Z-scheme WO$_3$/g-C$_3$N$_4$ composite photocatalyst with enhanced photocatalytic performance under visible light, Appl. Surf. Sci. 391 (2017) 202–210.

[186] Z. Wan, G. Zhang, X. Wu, S. Yin, Novel visible-light-driven Z-scheme Bi$_{12}$GeO$_{20}$/g-C$_3$N$_4$ photocatalyst: oxygen-induced pathway of organic pollutants degradation and proton assisted electron transfer mechanism of Cr(VI) reduction, Appl. Catal. B 207 (2017) 17–26.

[187] Z. Dong, Y. Wu, Magnetically separable photocatalyst of direct Z-scheme g-C$_3$N$_4$ nanosheets/natural hematite ore hybrids, J. Photochem. Photobiol. A 336 (2017) 156–163.

[188] X. Liu, A. Jin, Y. Jia, T. Xia, C. Deng, M. Zhu, C. Chen, X. Chen, Synergy of adsorption and visible-light photocatalytic degradation of methylene blue by a bifunctional Z-scheme heterojunction of WO$_3$/g-C$_3$N$_4$, Appl. Surf. Sci. 405 (2017) 359–371.

[189] X. Zhao, J. Yu, H. Cui, T. Wang, Preparation of direct Z-scheme Bi$_2$Sn$_2$O$_7$/g-C$_3$N$_4$ composite with enhanced photocatalytic performance, J. Photochem. Photobiol. A 335 (2017) 130–139.

[190] J. Ding, Z. Dai, F. Qin, H. Zhao, S. Zhao, R. Chen, Z-scheme BiO$_{1-x}$Br/Bi$_2$O$_2$CO$_3$ photocatalyst with rich oxygen vacancy as electron mediator for highly efficient degradation of antibiotics, Appl. Catal. B 205 (2017) 281–291.

[191] Y. Meng, Y. Hong, C. Huang, W. Shi, Fabrication of novel Z-scheme InVO$_4$/CdS heterojunctions with efficiently enhanced visible light photocatalytic activity, CrystEngComm 19 (2017) 982–993.

[192] W. Zhu, F. Sun, R. Goei, Y. Zhou, Construction of WO$_3$-g-C$_3$N$_4$ composites as efficient photocatalysts for pharmaceutical degradation under visible light, Catal. Sci. Technol. 7 (2017) 2591–2600.

[193] X. Zhu, J. Liu, Z. Zhao, J. Yan, Y. Xu, Y. Song, H. Ji, H. Xu, H. Li, Hydrothermal synthesis of mpg-C$_3$N$_4$ and Bi$_2$WO$_6$ nest-like structure nanohybrids with enhanced visible light photocatalytic activities, RSC Adv. 7 (2017) 38682–38690.

[194] X. Ye, S. Zhao, S. Meng, X. Fu, L. Bai, Y. Guo, X. Wang, S. Chen, Remarkable enhancement of photocatalytic performance via constructing a novel Z-scheme KNbO$_3$/Bi$_2$O$_3$ hybrid material, Mater. Res. Bull. 94 (2017) 352–360.

[195] L.V. Bora, R.K. Mewada, Photocatalytic treatment of dye wastewater and parametric study using a novel Z-scheme Ag$_2$CO$_3$/SiC photocatalyst under natural sunlight, J. Environ. Chem. Eng. 5 (2017) 5556–5565.

[196] Q. Meng, H. Lv, M. Yuan, Z. Chen, Z. Chen, X. Wang, In situ hydrothermal construction of direct solid-state nano-Z scheme BiVO$_4$/pyridine-doped g-C$_3$N$_4$ photocatalyst with efficient visible-light-induced photocatalytic degradation of phenol and dyes, ACS Omega 2 (2017) 2728–2739.

[197] P. Meng, H. Heng, Y. Sun, X. Liu, In situ polymerization synthesis of Z-scheme tungsten trioxide/polyimide photocatalyst with enhanced visible-light photocatalytic activity, Appl. Surf. Sci. 428 (2018) 1130–1140.

[198] M. Sun, Y. Wang, Y. Shao, Y. He, Q. Zheng, H. Liang, T. Yan, B. Du, Fabrication of a novel Z-scheme g-C$_3$N$_4$/Bi$_4$O$_7$ heterojunction photocatalyst with enhanced visible light-driven activity toward organic pollutants, J. Colloid Interface Sci. 501 (2017) 123–132.

[199] X. Ma, W. Ma, D. Jiang, D. Li, S. Meng, M. Chen, Construction of novel WO$_3$/SnNb$_2$O$_6$ hybrid nanosheet heterojunctions as efficient Z-scheme photocatalysts for pollutant degradation, J. Colloid Interface Sci. 506 (2017) 93–101.

[200] C. Liu, Q. Wu, M. Ji, H. Zhu, H. Hou, Q. Yang, C. Jiang, J. Wang, L. Tian, J. Chen, W. Hou, Constructing Z-scheme charge separation in 2D layered porous BiOBr/graphitic C$_3$N$_4$ nanosheets nanojunction with enhanced photocatalytic activity, J Alloys Compd. 723 (2017) 1121–1131.

[201] B. Feng, Z. Wu, J. Liu, K. Zhu, Z. Li, X. Jin, Y. Hou, Q. Xi, M. Cong, P. Liu, Q. Gu, Combination of ultrafast dye-sensitized-assisted electron transfer process and novel Z-scheme system: AgBr nanoparticles interspersed MoO$_3$ nanobelts for enhancing photocatalytic performance of RhB, Appl. Catal. B 206 (2017) 242–251.

[202] P. Xia, B. Zhu, B. Cheng, J. Yu, J. Xu, 2D/2D g-C3N4/MnO2 nanocomposite as a direct Z-scheme photocatalyst for enhanced photocatalytic activity, ACS Sustain. Chem. Eng. 6 (2018) 965–973.

[203] T. Lv, D. Li, Y. Hong, B. Luo, D. Xu, M. Chen, W. Shi, Facile synthesis of CdS/

Bi$_4$V$_2$O$_{11}$ photocatalysts with enhanced visible-light photocatalytic activity for degradation of organic pollutants in water, Dalton Trans. 46 (2017) 12675–12682.

[204] K. Xu, J. Feng, Superior photocatalytic performance of LaFeO$_3$/g-C$_3$N$_4$ heterojunction nanocomposites under visible light irradiation, RSC Adv. 7 (2017) 45369–45376.

[205] M. Jourshabani, Z. Shariatinia, A. Badiei, Synthesis and characterization of novel Sm$_2$O$_3$/S-doped g-C$_3$N$_4$ nanocomposites with enhanced photocatalytic activities under visible light irradiation, Appl. Surf. Sci. 427 (2018) 375–387.

[206] T. Xiong, M. Wen, F. Dong, J. Yu, L. Han, B. Lei, Y. Zhang, X. Tang, Z. Zang, Three dimensional Z-scheme (BiO)$_2$CO$_3$/MoS$_2$ with enhanced visible light photocatalytic NO removal, Appl. Catal. B 199 (2016) 87–95.

[207] Z. Lei, W. You, M. Liu, G. Zhou, T. Takata, M. Hara, K. Domen, C. Li, Photocatalytic water reduction under visible light on a novel ZnIn$_2$S$_4$ catalyst synthesized by hydrothermal method, Chem. Commun. (2003) 2142–2143.

[208] S.L. Castro, S.G. Bailey, R.P. Raffaelle, K.K. Banger, A.F. Hepp, Nanocrystalline chalcopyrite materials (CuInS$_2$ and CuInSe$_2$) via low-temperature pyrolysis of molecular single-source precursors, Chem. Mater. 15 (2003) 3142–3147.

[209] B. Gao, L. Liu, J. Liu, F. Yang, Photocatalytic degradation of 2,4,6-tribromophenol on Fe$_2$O$_3$or FeOOH doped ZnIn$_2$S$_4$ heterostructure: insight into degradation mechanism, Appl. Catal. B 147 (2014) 929–939.

[210] D. Jiang, J. Li, C. Xing, Z. Zhang, S. Meng, M. Chen, Two-dimensional CaIn$_2$S$_4$/g-C$_3$N$_4$ heterojunction nanocomposite with enhanced visible-light photocatalytic activities: interfacial engineering and mechanism insight, ACS Appl. Mater. Interfaces 7 (2015) 19234–19242.

[211] W. Yuan, S. Yang, L. Li, Synthesis of g-C3N$_4$/CaIn$_2$S$_4$ composites with enhanced photocatalytic activity under visible light irradiation, Dalton Trans. 44 (2015) 16091–16098.

[212] P. Qiu, J. Yao, H. Chen, F. Jiang, X. Xie, Enhanced visible-light photocatalytic decomposition of 2,4-dichlorophenoxyacetic acid over ZnIn$_2$S$_4$/g-C$_3$N$_4$photocatalyst, J. Hazard. Mater. 317 (2016) 158–168.

[213] M.J. Islam, D.A. Reddy, N.S. Han, J. Choi, J.K. Song, T.K. Kim, An oxygen-vacancy rich 3D novel hierarchical MoS$_2$/BiOI/AgI ternary nanocomposite: enhanced photocatalytic activity through photogenerated electron shuttling in a Z-scheme manner, Phys. Chem. Chem. Phys. 18 (2016) 24984–24993.

[214] W.K. Jo, T.S. Natarajan, Fabrication and efficient visible light photocatalytic properties of novel zinc indium sulfide (ZnIn$_2$S$_4$) − graphitic carbon nitride (g-C$_3$N$_4$)/bismuth vanadate (BiVO$_4$) nanorod-based ternary nanocomposites with enhanced charge separation via Z-scheme transfer, J. Colloid Interfaces Sci. 482 (2016) 58–72.

[215] C. Yu, K. Wang, P. Yang, S. Yang, C. Lu, Y. Song, S. Dong, J. Sun, J. Sun, One-pot facile synthesis of Bi$_2$S$_3$/SnS$_2$/Bi$_2$O$_3$ ternary heterojunction as advanced double Z-scheme photocatalytic system for efficient dye removal under sunlight irradiation, Appl. Surf. Sci. 420 (2017) 233–242.

[216] M. Zhang, Y. Zhu, W. Li, F. Wang, H. Li, X. Liu, W. Zhang, C. Ren, Double Z-scheme system of silver bromide@bismuth tungstate/tungsten trioxide ternary heterojunction with enhanced visible-light photocatalytic activity, J. Colloid Interfaces Sci. 509 (2018) 18–24.